01 Nov 2023

Evaluation of Residual Flexural Behavior of Corroded Fiber-Reinforced Super Workable Concrete Beams

Jingjie Wei

Nima Farzadnia

Alfred Addai-Nimoh

Kamal Khayat
Missouri University of Science and Technology, khayatk@mst.edu

Recommended Citation

J. Wei et al., "Evaluation of Residual Flexural Behavior of Corroded Fiber-Reinforced Super Workable Concrete Beams," *Cement and Concrete Composites*, vol. 144, article no. 105278, Elsevier, Nov 2023. The definitive version is available at https://doi.org/10.1016/j.cemconcomp.2023.105278

Cement and Concrete Composites 144 (2023) 105278

Contents lists available at ScienceDirect

Cement and Concrete Composites

journal homepage: www.elsevier.com/locate/cemconcomp

Evaluation of residual flexural behavior of corroded fiber-reinforced super workable concrete beams

Jingjie Wei [a], Nima Farzadnia [a,b], Alfred Addai-Nimoh [a], Kamal H. Khayat [a,*]

[a] Department of Civil, Architectural and Environmental Engineering, Missouri University of Science and Technology, Rolla, MO, USA
[b] Department of Civil, Geological, and Environmental Engineering, University of Alaska Fairbanks, Fairbanks, AK, United States

ARTICLE INFO

Keywords:
Corrosion
Fiber-reinforced concrete
Macro synthetic fibers
Pre-crack width
Residual flexural behavior
Predicted model

ABSTRACT

This study investigates the effect of macro synthetic fiber (MSF) volume and crack widths on corrosion of the reinforcing bars and residual flexural behavior of fiber-reinforced super-workable concrete (FR-SWC) beams exposed to accelerated corrosion. FR-SWC beams prepared with 0, 0.33%, and 0.66% MSF were pre-cracked at 0.2-, 0.4-, and 0.75-mm widths before corrosion testing. The controlled crack width was initiated in one set of beams that were then unloaded. The crack width was maintained for another set of beams during corrosion testing by inserting a shim. Test results showed that the use of 0.33% and 0.66% MSF reduced crack development and crack propagation, delayed corrosion initiation time, and significantly increased the residual flexural strength of beams subjected to accelerated corrosion. The beams reinforced with 0.66% MSF enhanced residual ultimate load, residual yield load, and residual flexural toughness by 10%–45%, 38%–113%, and 42%–150% compared to the corresponding non-fibrous beams. The improved flexural performance of beams made with MSF after accelerated corrosion can be attributed to the ability of MSF to reduce crack width due to corrosion damage. Crack width lower than 0.2 mm showed no significant effect on the residual flexural behavior of beams after corrosion testing. However, the pre-crack width over 0.2 mm showed a significant influence on the crack initiation and residual flexural behavior after accelerating corrosion. The pre-cracked beams with a 0.75 mm crack width retained the ultimate load of 65%–76%, yield load of 47%–80%, and toughness of 38%–83%, respectively, compared to their corresponding uncracked beams subjecting to accelerated corrosion. The unshimmed beams allowed partial closure of cracks due to the presence of MSF after initial loading and increased the residual ultimate load, yield load, and flexural toughness by 7%–45%, 27%–82%, and 3%–56%, respectively, compared to their corresponding shimmed beams. A correlation between the residual flexural behavior and the rate of cross-sectional area loss of reinforcing bars due to corrosion was developed. Furthermore, a mechanism was proposed to explain the effect of MSF in improving the residual flexural performance in the cracked FR-SWC beams.

1. Introduction

Super-workable concrete (SWC) is a high-performance concrete (HPC) with adapted rheology that requires relatively low energy of consolidation compared to self-consolidating concrete (SCC) [1]. Due to its special rheological characteristics, SWC offers the majority of the benefits usually associated with SCC [2] while securing lower chemical admixture demand, greater robustness, and lower risk of segregation than SCC [3,4]. Although SWC has a lower paste content than SCC, binder volume is still higher than that of conventional vibrated concrete (CVC), hence necessitating shrinkage mitigation. Kassimi et al. [5] showed that the shrinkage of SWC can be 10%–35% higher than that of CVC. High shrinkage increases the cracking potential in concrete structures, which can lead to a greater risk of ingress of deleterious materials that can reduce the durability of concrete and increase the corrosion of reinforcing bars. Wang et al. [6] reported that the permeability in cracked concrete exhibited significantly higher than that of uncracked concrete. In general, the pre-existing cracks have a great influence on the flexural strength reduction of beams and the residual structural service life. Hoseinzade et al. [7] reported the role of cracks on the residual flexural capacity of reinforced concrete beams under a severe corrosion environment, showing that pre-existing cracks reduced

* Corresponding author.
E-mail address: kkhayat@mst.edu (K.H. Khayat).

https://doi.org/10.1016/j.cemconcomp.2023.105278
Received 22 May 2023; Received in revised form 1 August 2023; Accepted 31 August 2023
Available online 1 September 2023

residual flexural capacity by 11%–17% compared to similar uncracked beams. According to Bezuidenhou and Zijl [8], it has been noted that cracking factors, such as the number of cracks and crack spacing, can have an impact on the corrosion rate and initiation of reinforcing bars. These factors can diminish the residual service life of concrete structures.

The crack width also has a significant effect on the corrosion of reinforcing bars and residual flexural performance [9]. Fang et al. [10] reported that the increase in crack width from 0.2 to 0.4 mm can accelerate chloride ion ingress in the concrete leading to faster corrosion of reinforcing bars. However, a crack that was finer than 0.2 mm did not have a significant effect on the corrosion process [11]. The corrosion of steel reinforcement has an adverse effect on the residual flexural capacity of reinforced concrete beams. Yu et al. [12] reported that a 1% loss in the cross-sectional area of longitudinal reinforcing bars can lead to an approximately 1% decrease in relative yield strength and a 0.85% reduction in ultimate flexural capacity.

Fibers can reduce crack width due to shrinkage due to their bridging effect. Kassimi and Khayat [13] reported that the use of 0.5%–1.4% steel fiber, by volume, in SCC can reduce the crack width by 40%–56% compared to the plain SCC. Similar results were found by Passuello et al. [14] with crack width reduction of approximately 70% in concrete made with macro-fibers and 90% in concrete made with micro-fibers. Furthermore, the incorporation of fibers can enhance the residual strength and overall behavior of structural elements made with fiber-reinforced concrete (FRC). Teng et al. [15] reported that adding 1.2% steel fibers, by volume, can significantly improve the residual flexural strength showing a deflection-hardening behavior compared to the brittle behavior of the plain concrete. Lee and Won [16] demonstrated that the use of 0.4% structural synthetic and 0.25% steel fibers can increase the flexural load capacity by 30% compared to the designed ultimate load. Furthermore, Falara et al. [17] conducted a study on the impact of using multiple-scale carbon fiber on the flexural behavior of cement composites. The researchers found that adding 0.5% micro-scale carbon fibers and 0.1% nano-scale carbon fibers, by mass, in cement can lead to 56% increase in flexural strength compared to a similar mixture without fiber.

The use of fibers can effectively enhance the fracture characteristics, especially for the cracking resistance, of FRC samples compared to plain concrete. Ríos et al. [18] and Xie et al. [19] reported that fibers can provide a bridging effect on the crack front, hence reducing microcrack width and length and enhancing toughness, both for steel and synthetic fibers. Smarzewski [20] indicated that using 2% polypropylene (PP) fibers, by volume, exhibited 130% higher fracture energy than the HPC beam made with 0.5% PP fibers, demonstrating that the increase in PP fiber content can significantly improve the ability to retain cracks. A similar finding was reported in the previous study [21], demonstrating that fracture toughness increased by 57% as steel fiber content increased from 0 to 0.4%, by volume of concrete.

The detection of crack propagation is more challenging in the presence of fibers given the reduction of cracking and crack width. Detection methods to monitor the effect of fiber on cracking behavior have been developed. Voutetaki et al. [22] employed piezoelectric transducers (PTZ) to detect cracking in FRC. The method can monitor the changes in the signal of each PZT because of the variation in mechanical impedance caused by FRC cracking. The authors reported that incorporating 5% synthetic fibers, by volume, in concrete can reduce the variation in the signal of each PZT, which indicates the PTZ test can be an effective method to monitor FRC cracking. Mpalaskas et al. [23,24] showed that waveform parameters of the acoustic emission (AE) can offer real-time monitoring of crack propagation, which enables the characterization of the critical moments of the structure in relation to the applied load. Additionally, Paul et al. [25] found that the application of AE in FRC can be a good option to analyze crack growth, crack location, as well as matrix cracking and fiber slippage.

Steel fibers are widely used to mitigate cracking and reduce crack width, improve crack propagation resistance, and flexural properties [10,26–28]. In some cases, the use of steel fibers can accelerate corrosion of reinforcing bars embedded in concrete exposed to a corrosive environment [29,30]. For example, Roque et al. [31] investigated the effect of fiber type on the corrosion resistance of reinforcing bars in FRC (water to cementitious materials ratio of 0.44) subjected to a corrosion environment for 27 months. The results reported that the time of initial corrosion of embedded steel rebar in samples cast with steel fibers took place 54 days earlier than that of the plain concrete (191 vs. 137 days, which corresponds to 28% spread of time). Similar results were found by Kim et al. [32], who reported that the time of initial corrosion of reinforcing bars in concrete made with steel fibers can be about 100 days earlier than that in plain concrete.

Macro synthetic fibers (MSF), also known as structural fibers, are alternatives to improve crack resistance and the structural performance of reinforced concrete. The overall performance of MSFs in terms of serviceability, load carrying capacity, ductility, and crack control of deep beam samples made with 2% MSF fibers, by volume of concrete, is reported to be superior to that of the plain reinforced concrete samples and reinforced concrete samples with 1% of steel fiber [33]. The use of MSF fiber showed similar efficiency in improving the shearing capacity and post-cracking behavior of prestressed concrete beams under flexure-shear compared to similar elements made with steel fibers [34,35]. Bicer et al. [36] investigated the effect of PP fibers on the flexural strength of fiber-reinforced concrete (FRC) beams and proposed a new model to predict the flexural strength of FRC. The results indicated that the use of PP fibers can increase flexural performance, and the proposed model showed good agreement with current and previously published data.

Many studies show that the use of MSF fiber can provide superior post-crack control performance and effectively control crack width due to the geometry and elastic modulus [37–39]. The addition of MSF fiber can significantly improve the post-cracking stiffness of beams and reduce crack widths at service loads [40]. The increase in post-cracking stiffness varied from 30% to 79% for FRC beams made with MSF fiber used at 0.35%–1.0%, by volume [41]. Moreover, the crack widths can decrease significantly at service loads with the increase in MSF volume [41]. The post-crack control performance of MSF fiber can reduce the risk of cracking, enhance the corrosion resistance of reinforcing bars and increase the residual performance of cracked beams. As expected, the use of MSF fiber should not promote any micro-cells that can increase the risk of corrosion of reinforcing steel [42].

FRC members subjected to high levels of stress can crack. In some cases, cracking can exceed serviceability levels leading to larger cracks. However, cracks can partially close upon load removal, especially in FRC that can limit the propagation of cracks and reduce crack widths. There is a lack of information on the effect of crack width on the corrosion of reinforcing bars in the presence of MSF. Limited studies also exist on the effect of MSF type, fiber geometry, and fiber factor on the residual flexural performance of cracked elements having different crack widths. Therefore, this study aims to investigate the effect of using MSF on enhancing the corrosion resistance of reinforcing bars embedded in fiber-reinforced super workable concrete (FR-SWC) beams subjected to different crack widths before exposure to accelerated corrosion testing. The combined influence of MSF fiber volume and pre-cracked width on the residual flexural behavior of beams is also investigated. A total of 24 notched beams prepared with MSF content of 0, 0.33%, and 0.66%, by volume, were investigated. The beams were pre-cracked to secure initial crack widths of 0.2, 0.4, and 0.75 mm before the accelerated corrosion testing. The electrochemical tests were conducted to evaluate the crack initiation and reinforcing bar corrosion of cracked/uncracked beams. After the corrosion testing of 200 days, the four-point loading tests were conducted to assess the residual behavior of corroded FRC beams. The relationship between the residual behavior and the cross-section area loss rate of reinforcing bar was established after corrosion testing and a hypothesis was proposed to explain the effect of MSF fiber in improving

the residual performance in the cracked FR-SWC beams.

2. Experimental program

A schematic flow diagram illustrating the test procedure is shown in Fig. 1. 24 FR-SWC beams measuring 200 × 200 × 610 mm were cast. A notch with a depth of 10 mm and a width of 5 mm was formed at the mid-span of the beam to ensure pre-cracking at the mid-span. The beams were pre-cracked at various crack widths ranging from 0 to 0.75 mm and after that, the beams were then subjected to accelerated corrosion testing for 200 days. A notch with a dimension of 5 × 5 mm was saw-cut before conducting the residual flexural performance of the beams. Finally, the mass loss and cross-sectional area loss of the reinforcing bars was calculated.

2.1. Materials

Type I ordinary Portland cement (OPC) and Class C fly ash (FA) were used to prepare FR-SWC in this study. The river-bed siliceous sand with a fineness modulus of 2.59, a specific gravity of 2.62, and surface saturated dry (SSD) water absorption of 0.35% was used. Crushed limestone aggregate with a nominal maximum size of 12.5 mm and specific gravity of 2.72 was used. To mitigate the drying shrinkage of FR-SWC, a saturated lightweight sand (LWS) was utilized to provide internal curing. The SSD specific gravity and water absorption of the LWS are 1.83 and 17.5%, respectively.

Two types of MSF were used, MSF_1 and MSF_2, as shown in Fig. 2. The shape of the MSF_1 and MSF_2 is corrugated and straight, respectively. The MSF_1 and MSF_2 are made from two materials (polypropylene and polyethylene). The lengths, diameters, and aspect ratios of the MSF_1 are 50 mm, 0.68 mm, and 75, respectively. Such values are 32 mm, 0.43 mm, and 75, respectively, for the MSF_2. According to the tensile testing of single fiber, the tensile strengths and elastic moduli of MSF_1 and MSF_2 are 550 and 620 MPa, and 7 and 9 GPa, respectively.

A shrinkage-reducing admixture (SRA) was used to reduce the drying shrinkage of the SWC. The SRA was a clear liquid admixture with a density of approximately 0.92 kg/L. A polycarboxylate-based superplasticizer (SP), a water-soluble viscosity-modified admixture (VMA), and a synthetic resin-based air-entraining admixture (AEA) were introduced into the mixture to enhance flowability, resistance to segregation, and improve the frost durability of the concrete. The solid content of SP, VMA, and AEA are 20%, 15.8%, and 10.7%, respectively, and their specific gravities are 1.1, 1.03, and 1.02, respectively.

A No. 4 steel reinforcing bar with a nominal diameter of 12.7 mm

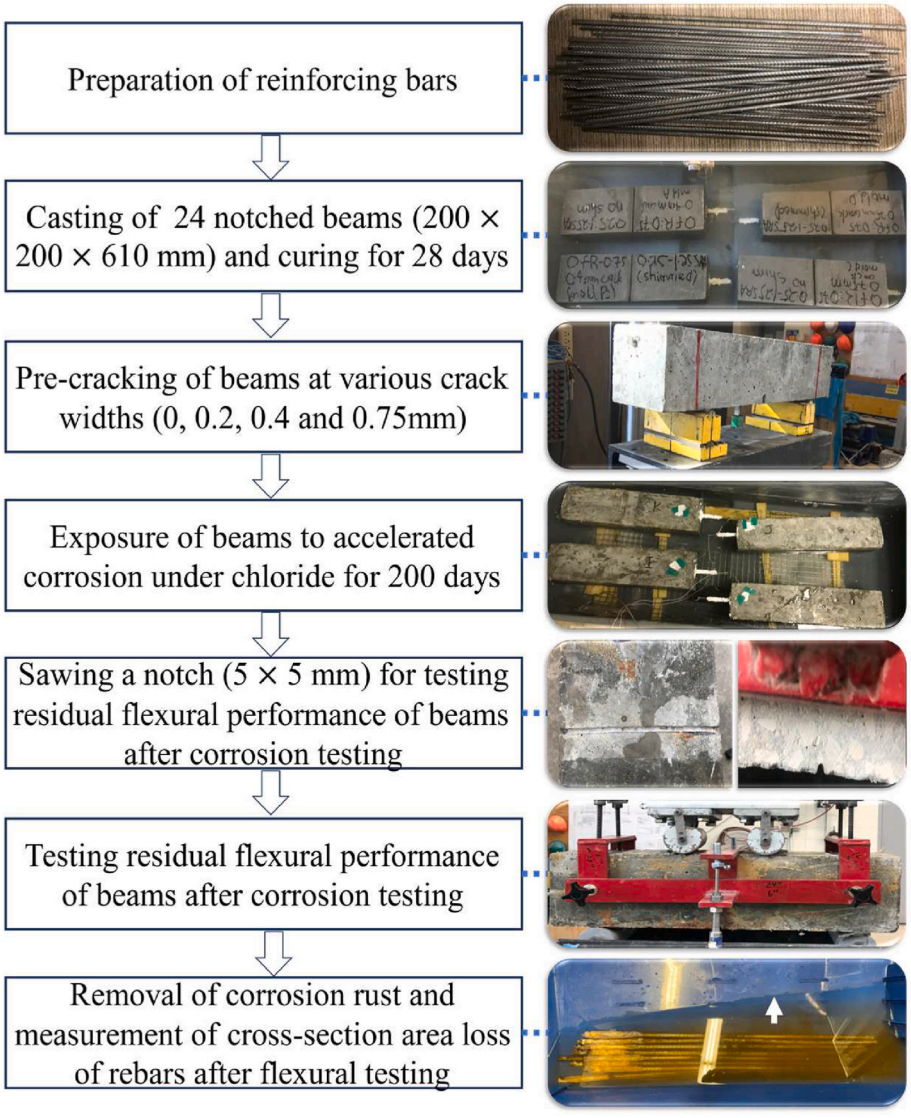

Fig. 1. Schematic of experimental programs.

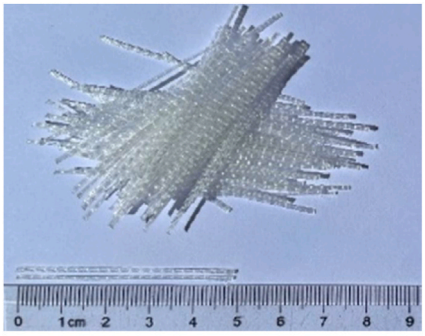

Macro synthetic fiber 1 (MSF_1)

Macro synthetic fiber 2 (MSF_2)

Fig. 2. Two macro synthetic fibers.

was used for the preparation of the test beams subjected to corrosion testing. The weight per unit length and nominal area of the bar is 0.996 kg/m and 129 mm^2, respectively. The tensile tests conducted on the reinforcing steel bar revealed a yield stress of 546 MPa, an ultimate strength of 626 MPa, an ultimate strain of 12%, and an elastic modulus of 204 GPa.

2.2. Mixture proportion and mixing procedure

Table 1 shows the details of the FR-SWC mixture proportions. Three FR-SWC mixtures made with 0%, 0.33%, and 0.66% fiber contents, by volume, were prepared to investigate the effect of MSF volume on corrosion resistance. A hybrid system of 75% MSF_1 and 25% MSF_2 was utilized for the FR-SWC mixture, based on the pre-experimental results which showed an enhancement in shrinkage mitigation and mechanical properties. In this study, the incorporation of 1.25% polyether type-based SRA, by mass of binder, was employed to mitigate drying shrinkage. To achieve better placement efficiency and workability, the initial slump flow of the FR-SWC was maintained at 500 ± 50 mm by adjusting the polycarboxylate ether-based SP demand (2.1–7.0 L/m^3). Higher dosages of VMA made with welan gum were required for the mixtures with high volume of synthetic fibers. The VMA dosage ranged between 3.3 and 10.4 L/m^3 to control the stability of the concrete. The investigated FR-SWC mixtures had a water-to-binder ratio of 0.43 and a binder composition consisting of 70% Type I cement and 30% FA, by mass. As shown in Table 1, the Ref. mixture corresponds to the mixture without any fiber. The codification of 0.33FR corresponds to the concrete beam cast with FRC of a volume of 0.33% MSF, while the 0.66FR beam was made with 0.66% MSF.

Concrete mixtures were prepared using a 150-L capacity drum mixer. The sand and pre-saturated LWS were thoroughly mixed together for a duration of 30 s to ensure homogeneity. Then the coarse aggregate and MSF were mixed for 2 min. Half of the mixing water with the diluted AEA was then added gradually to the mixer for over 1 min. The cement and FA were introduced to continue mixing for 1 min. The remaining 1/4 of the mixing water with 3/4 of the SP was mixed over 1 min. Finally, the remaining 1/4 of the mixing water with the VMA was mixed for 3 min. The remaining 1/4 of SP was used to secure the target slump flow of 500 ± 50 mm and mixer for 2 min. Finally, the SRA was introduced, and the concrete was remixed for 2 min.

In this study, compressive strength (100 × 200 mm cylinders), flexural strength (75 × 150 × 405 mm prisms), drying shrinkage (285 × 75 × 75 mm prisms), and bulk electrical resistivity (100 × 200 mm cylinders) of FR-SWC were evaluated. All samples were cast in one layer, rodded 10 times, and tapped 10 times using a rubber mallet. The samples were cured for 24 h in the mold under wet burlap, then de-molded after one day and cured in lime-saturated water at 23 ± 2 °C for 6 days. All samples for compressive strength, flexural strength, and bulk electrical conductivity were then transferred to the curing chamber and kept at 23 ± 2 °C and 50% ± 5% relative humidity until the testing age.

2.3. Materials characterization tests

A compressive strength test was carried out according to the ASTM C39 [43]. The loading rate was controlled to secure compressive stress of 0.25 ± 0.05 MPa/s. Drying shrinkage was evaluated according to ASTM C157 [44] with the initial length determined at 1 d of age. The electrical resistivity was determined on cylindrical samples at 28 days using the ASTM C1760 [45] and AASHTO TP 95–11 [46] standards. The direct two-electrode method was utilized to evaluate bulk electrical conductivity, while the four-point Wenner probe method was employed to measure surface resistivity.

2.4. Notched beam and control cracking

2.4.1. Preparation of notched beams

The investigated beams measured 610 mm in length with a cross-sectional of 200 × 200 mm, as shown in Fig. 3. The beams were reinforced with a No. 4 ribbed reinforcing bar with a nominal diameter of 12.7 mm that was positioned with a concrete cover clearance of 30 mm. Prior to concrete casting, the surface of the reinforcing bar was meticulously sandblasted to eliminate any mill scale. To establish an electrical connection, one end of the reinforcing bar was drilled and tapped, allowing for the insertion of a screw and ring terminal. Furthermore, both ends of the reinforcing bar were coated with a layer of moisture sealant and securely wrapped with electrical tape. A notch with a depth

Table 1
Mixture proportions of FR-SWC.

Mixture	OPC (kg/m^3)	FA, (kg/m^3)	Water (kg/m^3)	CA (kg/m^3)	Sand (kg/m^3)	LWS, (kg/m^3)	SRA (kg/m^3)	SP (L/m^3)	VMA (L/m^3)	Fiber (kg/m^3)	
										MSF_1	MSF_2
Ref.	255	110	148	800	728	172	4.56	2.1	3.3	0	0
0.33FR	255	110	147	751	757	178	4.56	2.6	3.3	2.3	0.7
0.66FR	255	110	138	703	786	185	4.56	7	10.4	4.5	1.5

Note: OPC: Type I cement; FA: fly ash; LWS: lightweight sand; SRA: shrinkage-reducing admixture; CA: coarse aggregate; SP: superplasticizer; VMA: viscosity modified admixture.

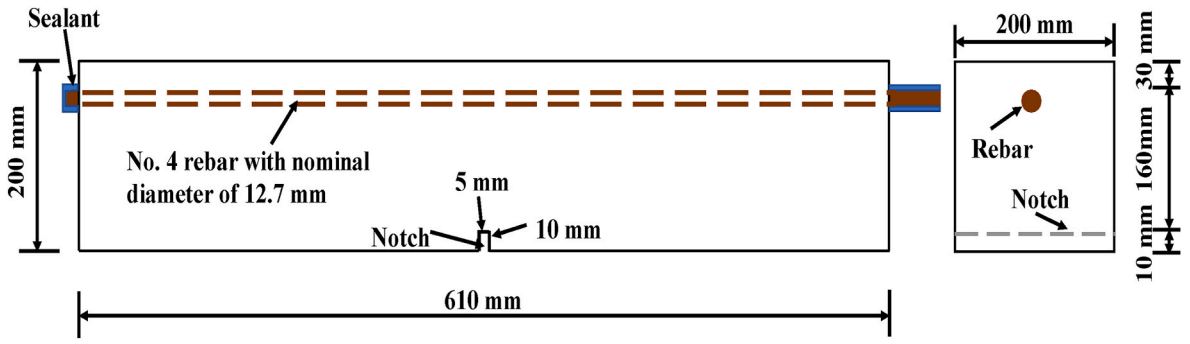

Fig. 3. Geometry of the notched beam.

of 10 mm and a width of 5 mm was formed at the mid-span of the beam. The purpose of the notch was to ensure that cracking can take place at a notch location. For the FR-SWC beams, the casting was in one layer, and consolidation was carried out using the vibrating table for 20 s. The notched beams were cured for 24 h in their molds under wet burlap, and they were then de-molded, and cured in lime-saturated water at 23 ± 2 °C for 28 days.

2.4.2. *Pre-loading procedure*

The notched beams were pre-cracked at the age of 28 days subjecting them to four-point loading flexural testing (i.e. third-point bending test) at a loading rate was 0.01 mm/min (Fig. 4). The distance between the upper rollers of the load cell was 100 mm. During the pre-loading procedure, the surface crack width on each reinforced beam was carefully monitored using an epsilon clip gauge with a 0.01 mm resolution. This precise measurement method allowed for the determination of when the desired crack width was achieved. The loading was stopped when crack widths reached various stages. After removing the load, the variation of the residual crack width was from 0.03 to 0.08 mm. The pre-cracks for the beams cast with FR-SWC did not reach the reinforcing bar.

As in [10,47–49], the crack width of 0.2 mm is generally taken as the threshold crack width for reinforcing bar corrosion. According to ACI 224R-08 [50], a crack width of 0.4 mm is considered the maximum allowable width below which a reinforced concrete structure might remain unaffected, and no repair is needed. The 0.75 mm crack width was selected to simulate adverse crack widths and may pose a severe corrosion threat to the concrete structure [51–54]. Therefore, the pre-crack widths were set at 0, 0.2, 0.4, and 0.75 mm, respectively. Two beams with the targeted pre-crack width were prepared for each mixture. One beam used a PVC shim at the location of the notch to maintain the initial crack widths during corrosion testing, while the other one did not, thus allowing cracks to close partially. The range of load and displacement at different pre-crack widths in the beams made with the Ref., 0.33FR, and 0.66FR concrete mixtures ranged from 0 to 22.15 kN and 0–0.19 mm, 0–25.05 kN and 0–0.25 mm, as well as 0–32.53 kN and 0–0.37 mm, respectively, as the crack widths on beams reached the target crack widths. Table 2 summarizes the pre-cracked beam schedule including the targeted crack widths, type of residual opening (shimmed or allowed to close after loading removal), load at cracked widths for shimmed and non-sustained cracks, crack widths after unload, displacement at crack widths, and crack length took place at the notch for all beams.

2.5. *Exposure conditions and corrosion monitoring*

All notched beams were immersed in water for one week after finishing the preloading procedure. Subsequently, the concrete beams were coated with epoxy to prevent the ingress of chloride ions through the concrete, except in the pre-crack area. Approximately one-third of the beam length was immersed in a 5% NaCl solution. As shown in Fig. 5, an electrical connection was made between the reinforcing bar and the stainless-steel mesh using a 5 V DC power supply and a 1-Ω resistor. With the stainless-steel mesh acting as the anode, and the reinforcing bar acting as the cathode, the voltage drop across the resistors over time was measured and using a multimeter to determine the current. The concentration of 5% NaCl in the solution was monitored every two weeks, and to maintain this concentration, all tanks were covered using a polyethylene sheet. The exposure period was over 200 days.

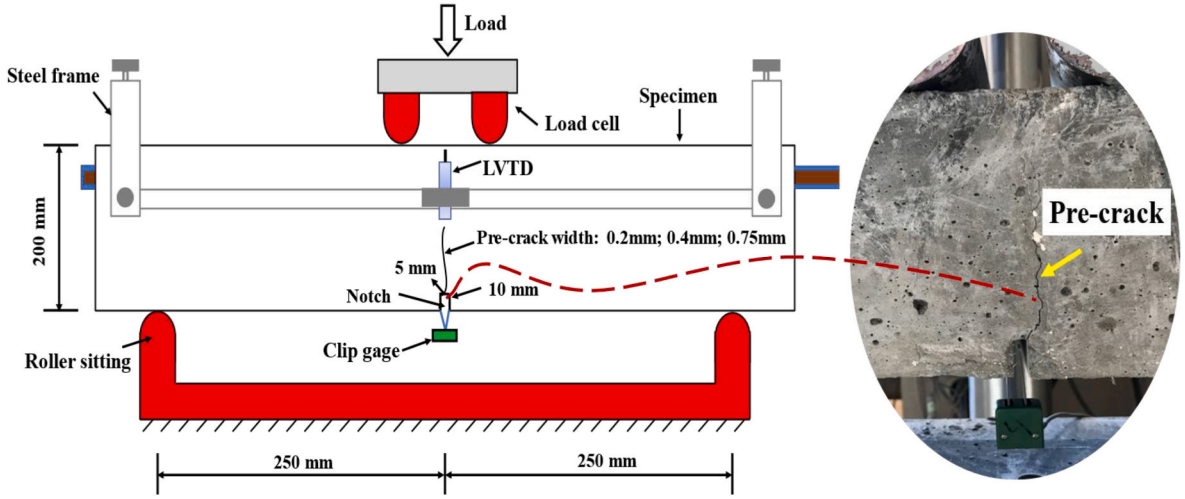

Fig. 4. Setup of flexural test used for pre-loading.

Table 2
Summary of the pre-cracked program for all notched beams.

Concrete mixture	Expected crack width (mm)	Type of crack opening	Load at crack width (kN)	Crack width after unloading (mm)	Displacement at crack width (mm)	Crack length (mm)	Concrete mixture	Expected crack width (mm)	Type of crack opening	Load at crack width (kN)	Crack width after unloading (mm)
		1	2	1	2	1	2	1	2	1	2
Ref.	0	No shim	No shim	0	0	0	0	0	0	0	0
	0.2	Shim	No shim	18.75	19.85	0.2	0.18	0.09	0.12	158	157
	0.4	Shim	No shim	21.09	21.55	0.4	0.39	0.13	0.14	160	161
	0.75	Shim	No shim	22.15	21.95	0.75	0.73	0.19	0.17	169	167
0.33FR	0	No shim	No shim	0	0	0	0	0	0	0	0
	0.2	Shim	No shim	20.05	21.75	0.2	0.15	0.15	0.17	150	149
	0.4	Shim	No shim	22.12	23.85	0.4	0.36	0.22	0.19	156	155
	0.75	Shim	No shim	24.95	25.05	0.75	0.60	0.25	0.24	157	158
0.66FR	0	No shim	No shim	0	0	0	0	0	0	0	0
	0.2	Shim	No shim	27.15	28.35	0.2	0.13	0.21	0.24	138	141
	0.4	Shim	No shim	29.25	30.41	0.4	0.33	0.29	0.31	145	148
	0.75	Shim	No shim	32.02	32.53	0.75	0.69	0.35	0.37	150	152

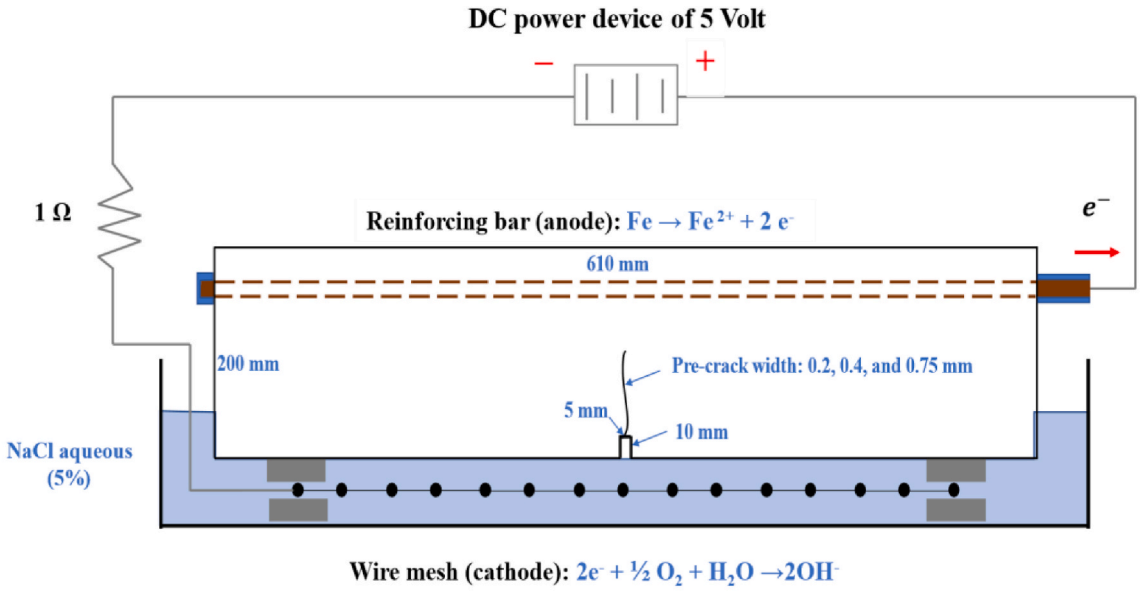

(a) Sketch of accelerated corrosion test setup (side view)

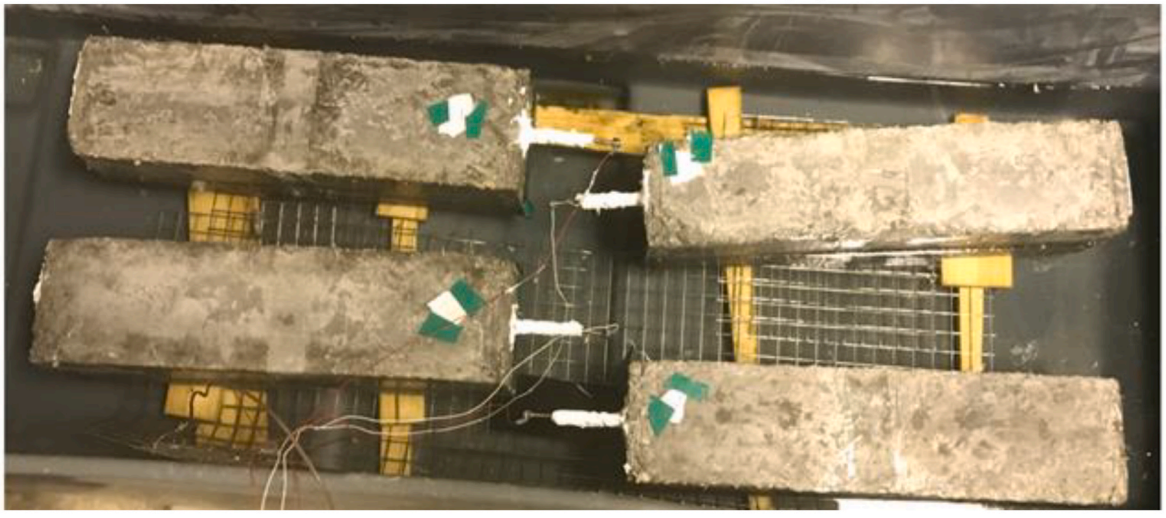

(b) Accelerated corrosion test (top view)

Fig. 5. Accelerated corrosion setup with 5 V supply.

2.6. Flexural tests

The pre-crack and the flexural testing of beam samples were tested by a three-point loading configuration, as shown in Fig. 6 in accordance with ASTM C1609. The reinforcing bar was located at the tension zone of the beams. An MTS 880 closed-loop testing machine with a load capacity of 1000 kN was used. The loading rate increased to secure at a displacement rate of 0.2 mm/min up to a mid-span displacement of 8 mm. The area within the flexural load-deflection curve between deflection values of 0 and L/150 (L is the span of the beam) was used to determine the dissipated energy or toughness. After the accelerated corrosion testing, a notch with 5 mm depth and 5 mm width was cut for flexural testing of concrete beams, as shown in Fig. 6.

2.7. Evaluation of reinforcing bar corrosion

Pre-cracking of FRC has a notable influence on the corrosion behavior of reinforcing bars. When cracks are wider, it becomes easier for corrosive agents to penetrate, resulting in accelerated corrosion. Investigating the relationship between pre-crack width and mass loss rate, as well as pre-crack width and cross-section area loss allows us to quantify this correlation and identify critical crack widths that have a significant impact on the corrosion of reinforcing bars embedded in FR-SWC beams. Furthermore, understanding this correlation enables us to evaluate the residual strength and long-term performance of corroded structures, facilitating more precise structural assessments and informed maintenance decisions.

The reinforcing bars were extracted from the beams after flexural tests and properly cleaned as outlined in ASTM G1-03 [55], to determine the mass loss of reinforcing bars due to corrosion as shown in Fig. 7. The mass loss was determined as follows: 1) the reinforcing bars were first cleaned with a wire brush and immersed in a solution made with 500 ml of hydrochloric acid, 3.5 g of hexamethylenetetramine, and 500 ml of water; 2) the weight of the reinforcing bars was determined after 30 min; 3) the procedure was repeated until there was no difference in weight.

The mass loss of the investigated reinforcing bars was used to assess the extent of corrosion. To determine the corrosion level, a precision scale with an accuracy of 0.001 g was used to measure the mass of the reinforcing bars. The mass loss rate of each reinforcing bar was then calculated as described in Equation (1):

$$m_{rl} = \frac{m_i - m_f}{m_i} \times 100 \tag{1}$$

where m_{rl}, m_i, and m_f refer to the mass loss rate (%), initial steel mass (g), and final steel masses (g), respectively.

The cross-section area loss of the reinforcing bar was used to evaluate the residual flexural performance of the FR-SWC beam subjected to an accelerated corrosion test. The initial and final cross-section areas of the reinforcing bars at the central point were calculated using the diameter of the reinforcing bars before and after the accelerated corrosion test. A vernier caliper with an accuracy of 0.01 mm was used to measure the diameter of the reinforcing bars. The cross-sectional area loss rate was calculated by Equation (2) as follows:

$$A_{rl} = \frac{\left(\pi\left(\frac{d_i}{2}\right)^2 - \pi\left(\frac{d_f}{2}\right)^2\right)}{\pi\left(\frac{d_i}{2}\right)^2} \times 100 \tag{2}$$

where A_{rl}, d_i, and d_f refer to the cross-sectional area loss rate (%), the initial diameter of reinforcing bars (mm), and the final steel diameter (mm) after the accelerated corrosion test, respectively.

3. Result and discussion

3.1. Concrete characterization

The effect of MSF volume on the workability, compressive strength, flexural strength, and drying shrinkage of FR-SWC is presented in Table 3. To enhance the reproducibility of the results, the values for mechanical properties, drying shrinkage, and electrical resistivity, are an average of three specimens. The slump flow and the air content of FR-SWC ranged from 470 to 550 mm, 5.0–6.5%. The higher air content in 0.66FR can be attributed to the agglomeration of fibers at a high-volume fraction. Compared to the Ref. sample, FR-SWC mixtures made with 0.33% and 0.66% MSF had slightly lower 56 d compressive strength (3% and 6% drop, respectively). The higher air volume can explain why the 0.66FR sample has lower compressive strength than the Ref. sample. Cavdar et al. [56] reported a similar result, showing the addition of 0.4%–1.2% synthetic fibers in concrete decreased the compressive strength by 8%–18% compared to the plain concrete. Similar results were reported by Fallah et al. [57], showing that the porosity of mixtures increased by 2%–4% when 0.5%–1.25% MSF was used in concrete.

The 56-d drying shrinkage of FR-SWC made with 0.33% and 0.66% MSF was 6% and 11% lower compared to the control sample. This is due to the restriction effect of MSF. The reduction in shrinkage is attributed

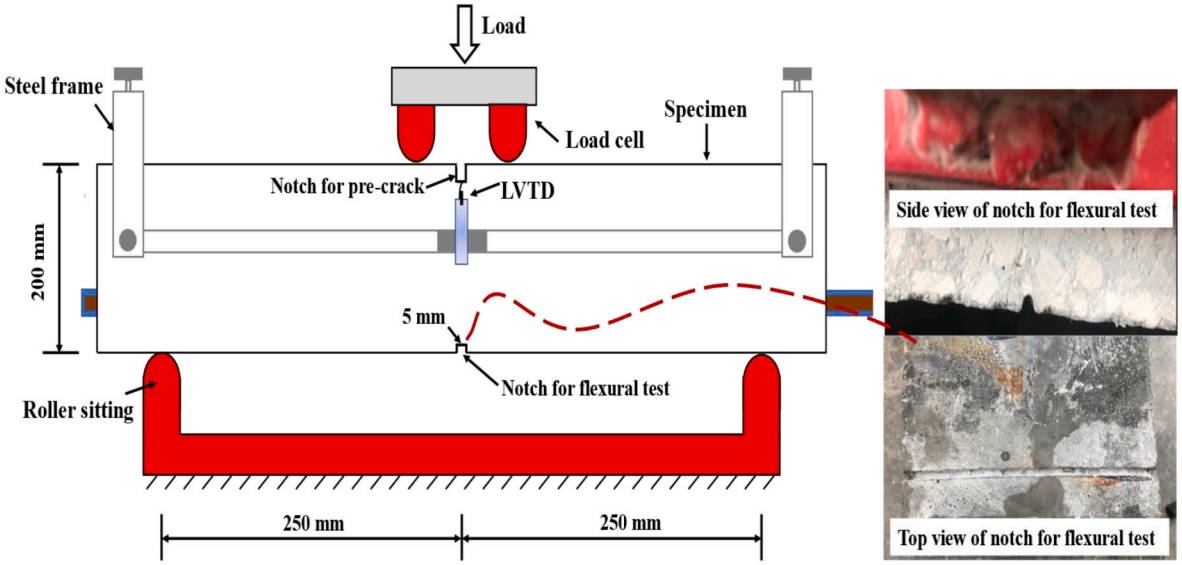

Fig. 6. Setup of flexural test after accelerated corrosion testing.

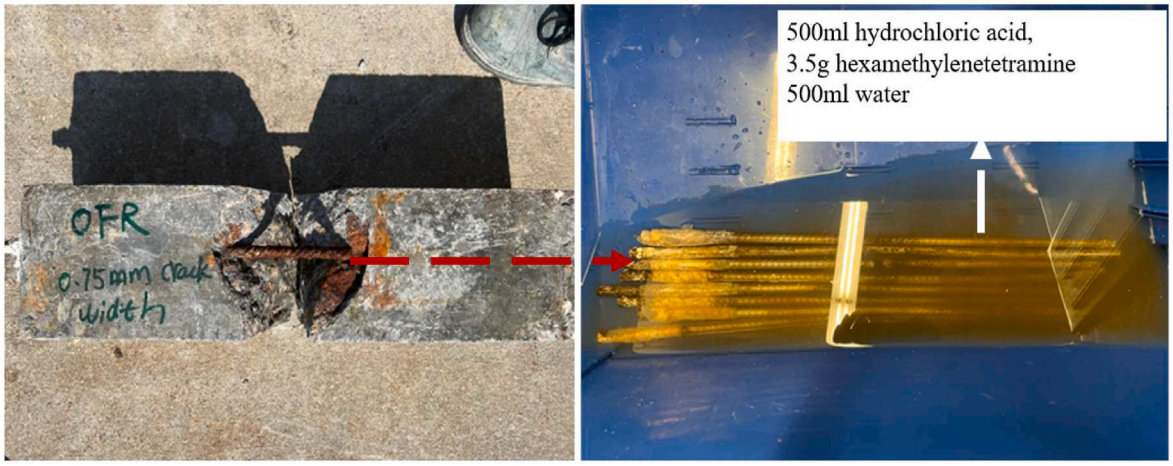

Fig. 7. Treatment process for evaluating mass loss of reinforcements after corrosion testing.

Table 3
Performance of FR-SWC mixtures.

Mixture	Slump flow (mm)	Air content (%)	56-d comp. strength (MPa)-(COV.)	56-d flexural strength (MPa)-(COV.)	56-d flexural toughness (kN.mm)- (COV.)	56-d Re,3-(COV.)	56-d drying shrinkage ($\mu\varepsilon$)–(COV.)	56-d bulk resistivity (kΩ.cm)- (COV.)	56-d surface resistivity (kΩ.cm)- (COV.)
Ref.	550	5.0	55.3 (3.7)	3.5 (2.9)	–	–	−401 (4.5)	243 (3.9)	82.4 (3.6)
0.33FR	515	5.3	53.6 (4.5)	4.0 (3.0)	8.8 (2.8)	39% (2.6)	−378 (4.6)	265 (4.2)	92.5 (3.8)
0.66FR	470	6.5	51.8 (3.4)	4.5 (3.2)	20.0 (3.2)	87% (3.5)	−356 (3.8)	150 (4.6)	64.5 (4.8)

to the tensile capacity of MSF that enable it to carry more tensile stress compared to plain concrete [58]. Similar results were reported by Karahan and Atis [59] where mixtures containing 0.05%–0.20% of synthetic fibers reduced drying shrinkage by 1%–11% compared to plain concrete. The bulk and surface resistivity of the 0.33FR sample increased by 9% and 12% compared to the plain concrete. Similar results were reported by Wang et al. [60] showing that concrete containing 0.5% macro-PP increased the bulk electrical resistivity by 10% compared to the plain sample. It was attributed to the electrical insulation property of a synthetic fiber that blocks the electrical transfer between two measure electrodes [61]. However, the bulk and surface resistivity of the 0.66FR mixture was reduced by 38% and 22%, respectively, compared to the Ref. sample. A similar result was reported in [61], showing that the concrete sample with 1.5% macro-PP decreased electricity resistivity by 20%–26% compared to the plain sample. Nili and Afroughsabet [62] reported a decrease in electrical resistivity as volume fractions of PP fibers increased by 0.5%. It was attributed to the fact that the addition of MSF caused the porosity of the mixture to increase [63], which can be verified by the increase in the air volume of the mixture and the reduction in compressive strength.

Fig. 8 shows the post-crack flexural behavior, including toughness and equivalent flexural strength ratio (Re,3) was greatly enhanced compared to the Ref. sample. Re,3 is the crack resistance ability. The improved crack resistance with the use of MSF is due to the physical properties of MSF and the ability to interlock with the matrix can reduce crack width [64]. The 0.66FR sample increased toughness and Re, 3 by 130% and 125% compared to the 0.33FR sample.

3.2. Corrosion-induced crack initiation

The crack initiation was determined by using the descent, steady, and ascent phases of the time-variant process of corrosion current [65], shown in Fig. 8. The descent phase of the current after the corrosion test can be related to the transporting rate of the aggressive ions (chloride ions, oxygen, and water) in the fiber-reinforced concrete matrix [66,67]. The corrosion current reaches a steady state when the rates of oxygen

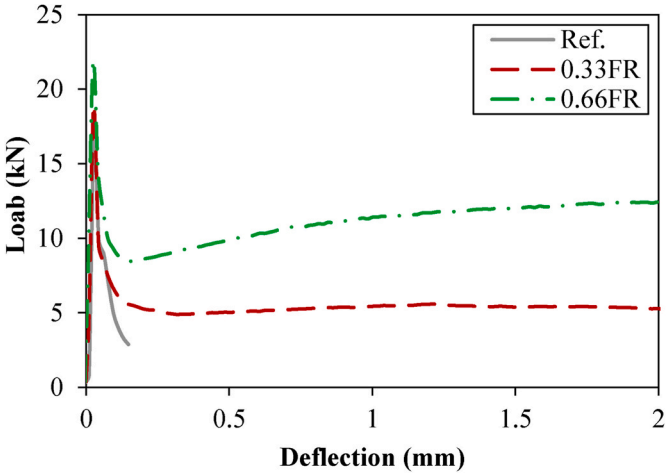

Fig. 8. Load-deflection of FR-SWC beams.

and water consumption and supply reach equilibrium, at which point it decreases to a certain level [68]. The ascent phase in the current is due to crack initiation caused by the expansive stresses caused by steel corrosion that exceed the tensile strength of the concrete. The cracking at the surface increases the content of OH^-, thus increasing the rate of corrosion product formation and current [69]. The typical current variation results of the reinforcing bar obtained from the corrosion test are shown in the descent, steady, and ascent phases. In the current variation diagram shown in Fig. 9, no surface corrosion-induced crack was observed in the descent and steady phases of the beam, which was the same for all other beams. The initiation of corrosion-induced cracking in all beams is located at the end of the steady phase and the start of the ascent phase.

As shown in Fig. 10, the MSF volume was an effective factor in the initiation time of the corrosion-induced cracks. In this study, the beams made with 0.33% MSF delayed the crack initiation by 3%–13%,

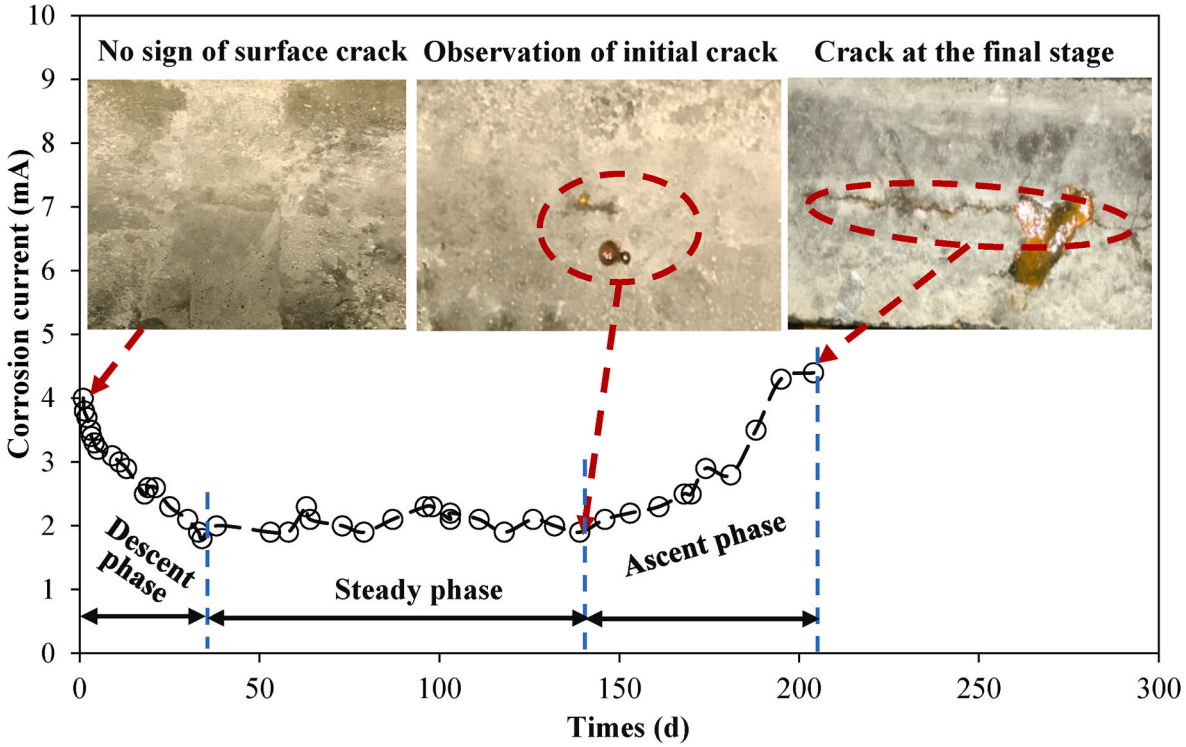

Fig. 9. Typical current variation of reinforcing bar in FR-SWC.

compared to the corresponding Ref. Beams. However, the beams made with 0.66% MSF did not further delay the crack initiation compared to the beams made with 0.33% MSF although beams made with 0.66% MSF delayed the crack initiation by 2%–8% compared to the corresponding Ref. Beams. As before mentioned, a high-volume fraction of MSF can lead to the "balling" effect and the agglomeration in the concrete matrix, resulting in a high permeability of the concrete matrix [70]. This can be verified by the result of bulk and surface resistivity in section 3.1. The high permeability of the concrete matrix increased the ingress of chlorides in the concrete. Therefore, the crack initiation of reinforcing bars in pre-cracked concrete beams made with 0.66% MSF showed at the early stage compared to beams made with 0.33% MSF.

The corrosion-induced cracks were initiated earlier with the increase of the pre-crack widths. The uncracked beams delayed the crack initiation by 19%–40% compared to beams with 0.75 mm pre-crack width. For example, as the pre-crack width increased from 0 to 0.75 mm, the mean time of crack initiation reduced from 175 to 110 d in the Ref. Beam, 180 to 119 d in the 0.33FR beam, and 177 to 115 d in the 0.66FR beam, respectively. It can be attributed to the ease of transportation of chloride ions to the interface between the reinforcing bar and concrete matrix through the relatively large cracks [52]. Cao et al. [71] reported that the corrosion degree of the reinforcing bar increased from 3% to 8% as the surface crack width increased from 0.2 to 1.0 mm, and the high corrosion degree resulted in earlier corrosion-induced cracks [72].

The reduction of crack width in the un-shimmed beams (i.e., cracks allowed to partially close after initial loading because of the presence of MSF) led to the delay of the crack initiation during the accelerated corrosion test [52]. The corrosion-induced crack initiation was delayed by 8%–20% and 12%–17% for the 0.33FR, and 0.66FR beams corresponding to similar beams that with shims at the notches Furthermore, the initiation of the corrosion-induced cracks in the 0.33FR and 0.66FR beams without shims was delayed by a maximum of 13% and 15%, respectively, compared to the non-fibrous beams without shims. This can be mainly attributed to the fact that the crack widths in all un-shimmed beams declined. This can be attributed to the fact that the use of MSF can help to bridge the crack, thus providing additional support to the two sides of the crack and restraint to the concrete matrix. As a result, when the load is removed, the use of MSF can help to bring the two sides of the crack closer together, allowing the crack to partially close.

3.3. Structural performance of cracked and uncracked beams

3.3.1. Load-deflection curves

Fig. 11(a)-(c) show the total applied load and mid-span deflection responses for FR-SWC beams made with 0%, 0.33%, and 0.66% MSF, respectively, before and after exposure to corrosion testing. It can be observed that the corrosion of reinforcing bars significantly influenced the flexural capacity of FR-SWC beams. The ultimate load of all corroded FR-SWC beams was lower than their corresponding unexposed beams. Specifically, the ultimate load of the exposed beams decreased by up to 50% compared to their corresponding unexposed beams. This can be attributed to the reduction in the cross-sectional area, the decrease in yield strength of the reinforcing steel bars, and the loss of bond strength between the corroded reinforcing bar and matrix [73,74].

The presence of MSF allows cracks to partially close after the initial load (i.e., un-shimmed beam), which shows a significant effect on the ultimate load of the pre-cracked beams after corrosion tests. The un-shimmed beam with a 0.75 mm crack width increased the ultimate load by 38% compared with its corresponding shimmed beams. This indicates that the use of MSF can inhibit crack propagation in the matrix, delaying the reinforcing bar corrosion in the same FR-SWC mixture. Furthermore, the ultimate load of the exposed beam (i.e., the beam subjected to accelerated corrosion testing) decreased with the increase in crack width. The Ref., 0.33FR, and 0.66FR samples with 0.75 mm decreased the ultimate load by 33%, 30%, and 24%, respectively, compared to their corresponding uncracked beams. This can be mainly attributed to the increase in crack width that increases the corrosion rate of the reinforcing bar, reducing the cross-sectional area of reinforcement [47]. Additionally, the residual ultimate load of 65%, 70%, and 76% in the Ref., 0.33FR, and 0.66FR samples with 0.75 mm crack width were

(a) Typical corrosion-induced initial crack

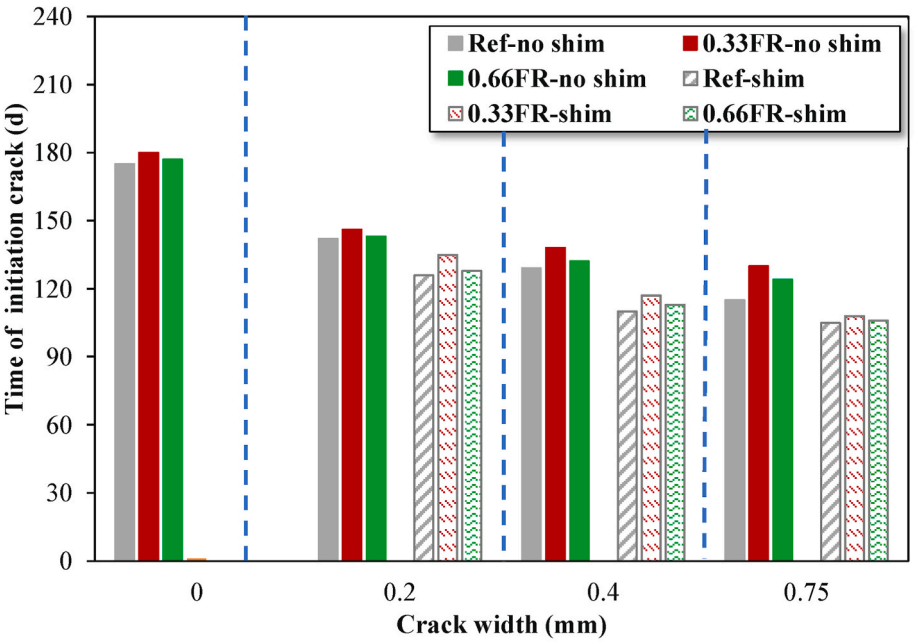

(b) Time of surface initial crack on beams

Fig. 10. Crack initiation on FR-SWC beams.

retained, respectively, after the accelerated corrosion test.

3.3.2. *Residual flexural capacity of exposed beams*

As shown in Fig. 12, the use of MSF inhibited crack development and increased the yield load of beams significantly. The beams reinforced with 0.33% and 0.66% MSF exhibited enhanced yield loads of 7%–58% and 38%–113% compared with the non-fibrous beams. This can be attributed to the superior post-crack performance of MSF leading to a significant increase in residual flexural performance [34,41,75]. The use of MSF also increases the tensile strength of concrete [76] and helps to distribute the load more evenly, which can improve its ability to resist the flexural load. Similar results were reported by Hammad et al. [77] where a reinforced concrete beam made with MSF can increase the yield load by 20% compared to the plain beam. The 0.66FR beam subjected to accelerated corrosion showed a higher yield load than the Ref. Beam. Furthermore, as expected, the increase in crack width showed a negative effect on the yield load of beams subjected to accelerated corrosion testing. As the crack width increased from 0 to 0.75 mm, the Ref., 0.33FR, and 0.66FR beams exhibited drops in yield load of 22%–53%, 17%–54%, and 7%–43%, respectively. This can be attributed to the fact that the increase in crack width reduced the cross-sectional area of the reinforcing bars, which decreases the load capacity of the reinforcing bar [47].

The yield load of shimmed or un-shimmed beams with different crack widths after accelerated corrosion tests was also compared. It can be observed that the yield load of the Ref. and 0.66FR beam with a 0.75 mm crack width decreased by 53% and 22% as compared with their corresponding uncracked beams. This can be attributed to the increase in pre-crack width of concrete beams that increased the corrosion rate of the reinforcing bar embedded in the concrete matrix and reduced its cross-section area, hence resulting in the reduction of the yield strength of the reinforcing bars [48]. Additionally, the yield load of un-shimmed beams was higher than those of shimmed beams. The yield load of un-shimmed beams reinforced with 0%, 0.33%, and 0.66% MSF increased by 27%, 82%, and 62%, respectively, compared with their corresponding shimmed beams. This can be mainly attributed to the higher crack widths in the shimmed beams compared to the un-shimmed beams, resulting in an increase of corrosion level and reduction of the cross-section area of the reinforcing bars.

Table 4 summarizes the residual flexural performance of the tested beams after the accelerated corrosion tests. The results showed that the flexural strength, mid-span moment, and toughness of all unexposed beams were higher than those of exposed beams, regardless of the fiber content, crack width, and the installed shim at the notch. This indicates the significant impact of the impaired properties of steel bars upon corrosion on the flexural capacity of the beam. Besides, for a given crack width, the flexural performance of the exposed beams increased with the increase in MSF volume. For example, at 0.75 mm pre-crack width, the

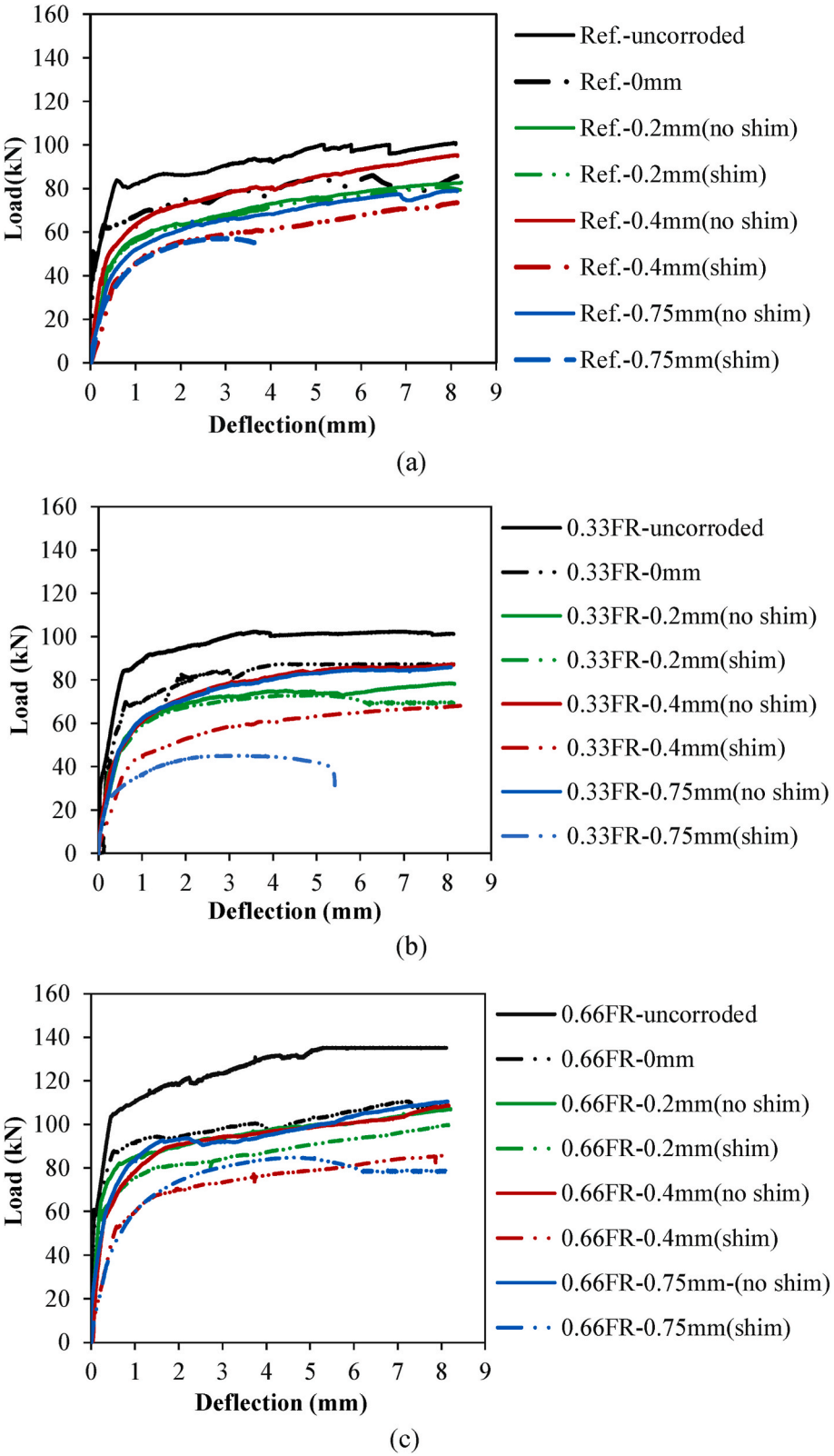

Fig. 11. Load-deflection of exposed beams:(a) Ref. beams; (b) 0.33%FR beams; (c) 0.66%FR beams.

flexural strength, moment, and flexural toughness of mixtures reinforced with 0.66% MSF exhibited a substantial increase of 42%, 45%, and 150%, respectively, in comparison to the non-fibrous beam. This significant improvement can be attributed to the bridging effect of MSF, which effectively mitigates the propagation of crack width, as shown in Fig. 13. However, the effect of MSF could not compensate for the negative effect of the corroded reinforcing bar, despite their significance on improving the flexural behavior of the exposed beams.

The pre-crack width lower than 0.2 mm showed no significant effect on the flexural toughness. This is because surface cracks lower than 0.2

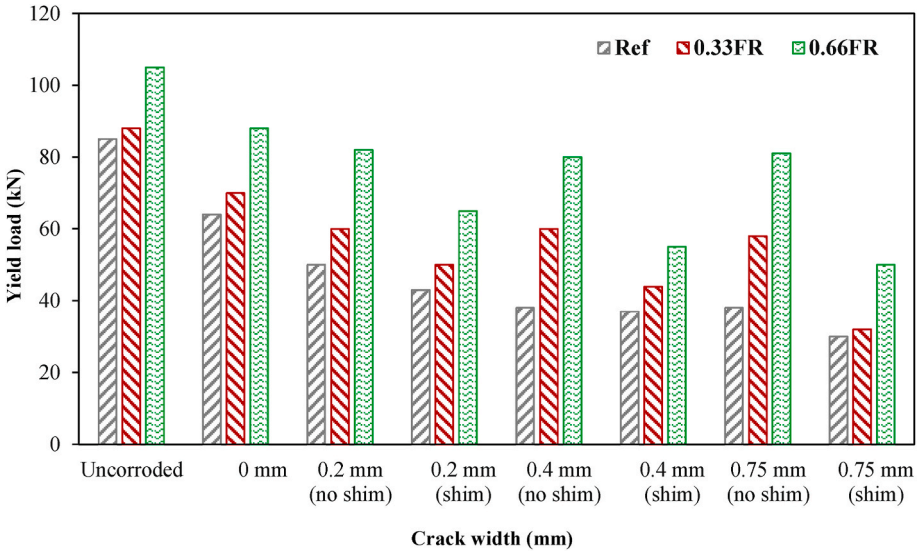

Fig. 12. Yield load of shimmed and un-shimmed beams at different crack widths.

Table 4
Summary of flexural test results.

Concrete type	Corrosion type	Cracked width (mm)	Flexural strength (MPa)		Moment (kN.mm)		Toughness (kN.mm^2)		Failure mode	
			Shim	No shim	Shim	No shim	Shim	No shim	Shim	No shim
Ref.	Unexposed	0	–	6.31	–	12625	–	710	–	Concrete
	Corroded	0	–	5.38	–	10750	–	520	–	Concrete
		0.2	5.00	5.25	10000	10375	480	530	Concrete	Concrete
		0.4	4.81	5.15	9625	11500	350	440	Concrete	Concrete
		0.75	3.63	5.00	7250	10000	200	312	Steel	Concrete
0.33FR	Unexposed	0	–	6.50	–	13000	–	805	–	Concrete
	Corroded	0	–	5.41	–	11020	–	550	–	Concrete
		0.2	4.95	5.29	9800	9875	500	560	Concrete	Concrete
		0.4	4.90	5.31	10800	10625	380	494	Concrete	Concrete
		0.75	3.68	5.25	9750	10500	252	343	Steel	Concrete
0.66FR	Unexposed	0	–	8.56	–	17125	–	1009	–	Concrete
	Corroded	0	–	6.88	–	13750	–	750	–	Concrete
		0.2	6.25	6.69	12500	13625	760	780	Concrete	Concrete
		0.4	5.31	6.75	10625	13500	740	700	Concrete	Concrete
		0.75	5.25	6.81	10500	12375	500	620	Concrete	Concrete

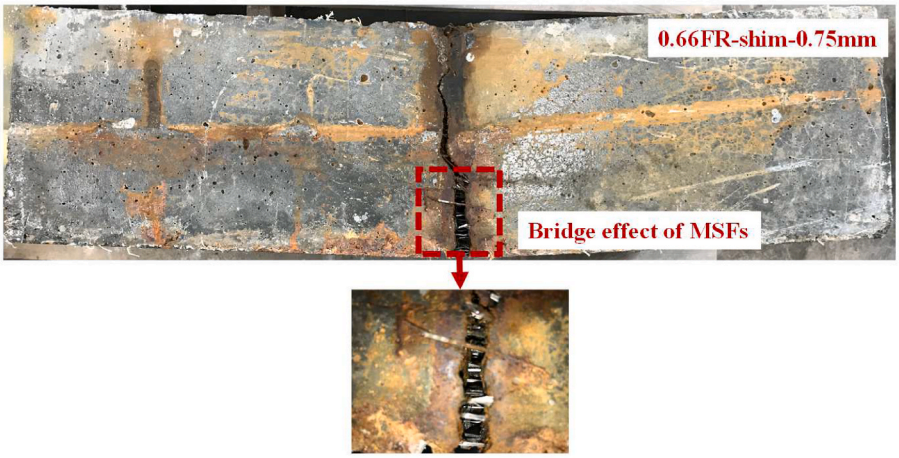

Fig. 13. Bridge effect of MSF at the notch for exposed beams.

mm can close over time, as shown in Fig. 14. Surface crack width less than 0.2 mm can be closed due to a process called autogenous healing, which occurs when moisture in the environment reacts with unhydrated cement particles in the concrete, forming calcium-silicate hydrates (*C*–S–H) that can fill the cracks and bond the two sides of the crack together [10,78]. The toughness of beams significantly decreased

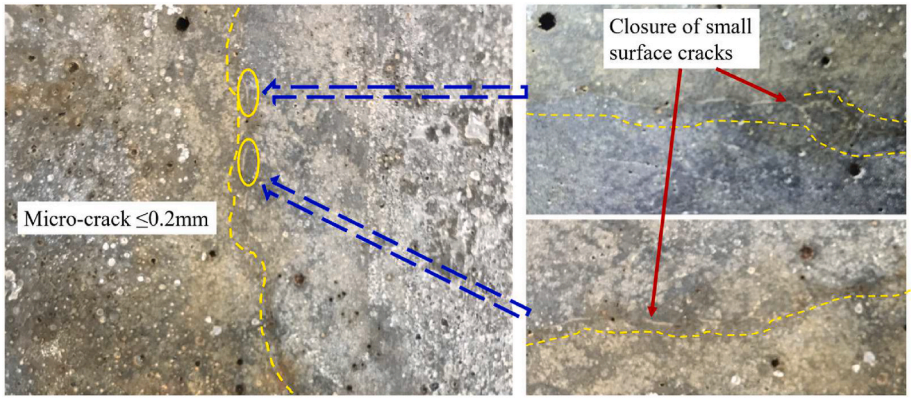

Fig. 14. Illustration of healing on the small crack surface (crack width ≤0.2 mm).

when the surface crack width was over 0.2 mm. The toughness of the Ref., 0.33FR, and 0.66FR beams with 0.75 mm crack width decreased by up to 62%, 54%, and 33%, respectively, compared with their corresponding uncracked beams. Furthermore, the flexural strength, mid-span moment, and toughness of un-shimmed beams are higher than shimmed beams, especially for beams reinforced with 0.66% MSF. The flexural strength, mid-span moment, and toughness of un-shimmed beams increased by up to 30%, 27%, and 24%, respectively, compared to shimmed beams. This can be attributed to the fact that the crack width of shimmed beams could not be decreased because the PVC shim sustained the crack width after removing the load and improved the corrosion of the reinforcing bar.

3.4. Visual observations

Fig. 15 shows the corrosion state of the reinforcing bar extracted from the beams. As shown in Fig. 15(a), the crack width lower than 0.2 mm did not show a significant reduction in the cross-section area of the reinforcing bar embedded in all beams. This was attributed to the fact that cracks lower than 0.2 mm can reduce the amount of water, oxygen, and Cl^- to reach the reinforcing bars [48]. Besides, the surface of the reinforcing bar at the center area only showed slight corrosion pits without serve damage to the rebar ribs. The rest of the reinforcing bars did not show visible corrosion pits. This observation indicated the locations of corrosion pits corresponded with the pre-crack width. On the other hand, as shown in Fig. 15(b), the cross-sections of the reinforcing bar at the center area significantly decreased when the crack width was over 0.2 mm, especially for the shimmed beams with 0.75 mm. This illustrated that more chloride ions can transport to the surface of the reinforcing bar through the wider crack (>0.2 mm), compared to the small crack (≤0.2 mm), resulting in severe corrosion of the reinforcing bar [10,47,49]. This is in agreement with the impaired toughness of

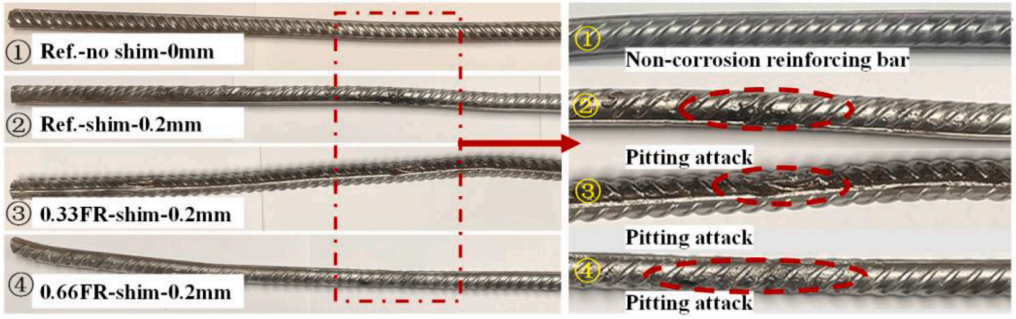

(a) Reinforcing bar embedded into concrete beam with pre-crack width lower than 0.2mm

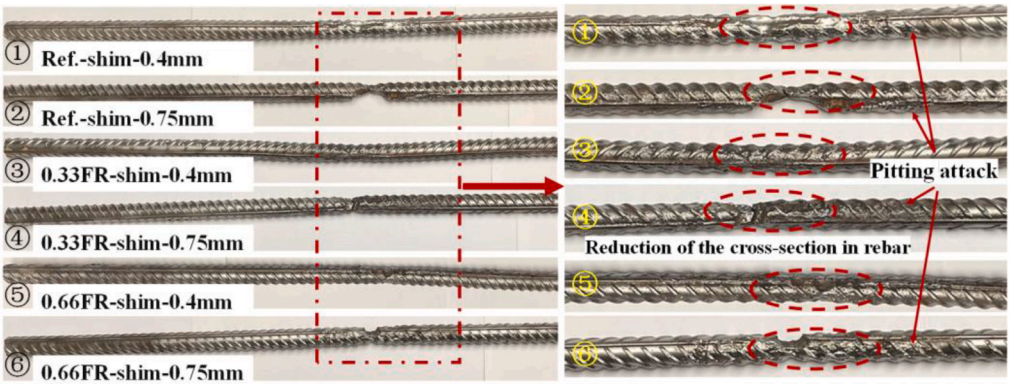

(b) Reinforcing bar embedded into concrete beams with pre-crack width over 0.2mm

Fig. 15. Typical corrosion pattern of reinforcing bar embedded in the FR-SWC beams.

beams as the crack width exceeds 0.2 mm. The reduction of the cross-section of the reinforcing bar at the center area was reduced with the increase in crack width. It is in agreement with the variation of residual flexural behavior of the beam. Furthermore, MSF showed a positive effect on the corrosion mitigation reinforcing bars as seen from the extent of corrosion of rebars. However, the beams with sustained crack width (shimmed notches) showed a reduction of the cross-section area of the reinforcing bar.

Fig. 16 shows the variation of the cross-sectional area of the reinforcing bars at the mid-span with the increase in pre-crack widths. For the beams with sustained crack width (shimmed notches), the cross-sectional area loss rate of the reinforcing bar rose from 23% to 83% as the pre-crack widths increased from 0 to 0.75 mm. However, such variations ranged from 15% to 57% for the beams with partial crack width closure (no shimmed notches). This can be attributed to the fact that the pre-cracks of no shimmed beams could be partially closed because of the crack control performance of MSF, improving the corrosion resistance of reinforcing bars.

3.5. Corrosion evaluation of reinforcing bar

Fig. 17 shows the mass loss rates of the reinforcing bars embedded in the cracked beams after the accelerated corrosion test. With an increase in pre-crack width, the rate of mass loss of the reinforcing bar increased. The mass loss rates of the Ref., 0.33FR, and 0.66FR beams increased from approximately 10%–13%, 9%–12%, and 10%–13%, respectively, as the crack width increased from 0 to 0.75 mm. In addition, shimmed beams showed 9% higher mass loss than un-shimmed beams. This can be attributed to the sustained crack width that can accelerate the rate of corrosion [79]. The use of MSF can reduce crack width and reduce the risk of corrosion [80]. For crack widths less than 0.4 mm, the reinforcing bar in the 0.33FR beam reduced the mass loss rate by up to 9%, whereas the 0.66FR beam increased the rate by up to 10%, relative to the Ref. Beam. This is consistent with the results of the bulk and surface resistivity results. However, for crack widths greater than 0.4 mm, the mass loss rate of the reinforcing bar in the 0.66FR beam decreased by 5% compared to the Ref. Beam. This was because the crack length can develop directly to the surface of reinforcement in the Ref. Beam, whereas the MSF in the 0.66FR beams prevented the crack length from propagating [81].

Table 5 summarizes the effect of MSF on the residual flexural behavior of beams and compares the tested data of previous studies on corrosion initiation delay and the mass loss rate of reinforcing bars, residual yield load, and residual ultimate load of exposed beams with three different fiber types (i.e., steel fibers, PP, and PE). The incorporation of fibers reduced reinforcing bar mass loss by 5%–61% and increased the residual yield and ultimate loads by 7%–113% and 4%–45%, respectively, compared to the plain beam. The use of fibers delayed the corrosion initiation of reinforcing bars by 4%–170% as compared to the plain concrete beam. Kim et al. [14] found that corrosion of bars can be accelerated by 55% in samples with steel fibers than in those with plain concrete. Early corrosion could be caused by chloride ions penetrating the concrete via micro-cracking caused by severely corroded steel fibers.

The use of MSF significantly increased the residual yield and residual ultimate loads of exposed beams compared to beams reinforced with steel fibers, while having a minimal impact on the mass loss rate of reinforcing bars. For instance, steel fibers increased the residual yield and ultimate load of the uncracked beam by 8%–21% and 8%–22%, respectively, after corrosion testing, despite significant improvement in flexural performance before corrosion. Compared to steel fibers, the use of MSF can develop proper resistance to corrosion and help to retain the residual flexural behavior of beams after being subjected to a corrosion environment. For instance, the use of MSF reduced the mass loss rate of reinforcing bars by a maximum of 12%, while the residual yield and ultimate load of uncracked beams reinforced with MSF increased by a maximum of 38% and 27%, respectively. Besides, using steel fibers improved the yield and ultimate load of cracked beams by 8%–17% and 6%–11%, respectively, compared to the plain concrete beam, while such values were 113% and 45% in cracked beams made with MSF. This suggests that in a corroded environment, microcracks can accelerate the corrosion of steel fibers and reinforcing bars, resulting in a more significant reduction in flexural performance.

Similar results were observed in beams reinforced with other synthetic fibers when the use of PP and PE increased the maximum yield and ultimate loads in uncracked beams by 21% and 28%, 43%, and 44%,

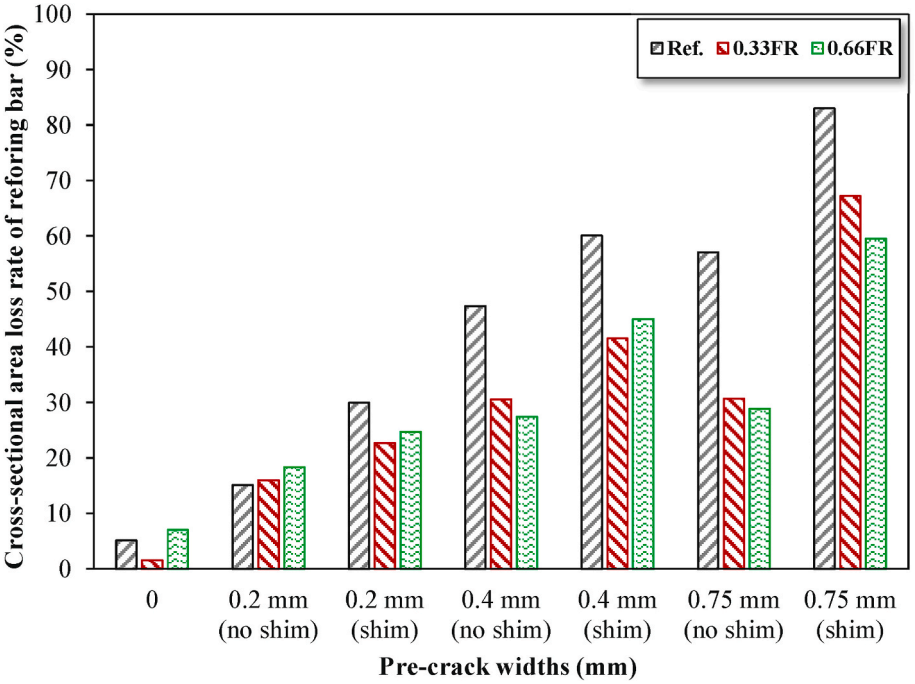

Fig. 16. Cross-sectional area loss rate of reinforcing bars at different crack widths.

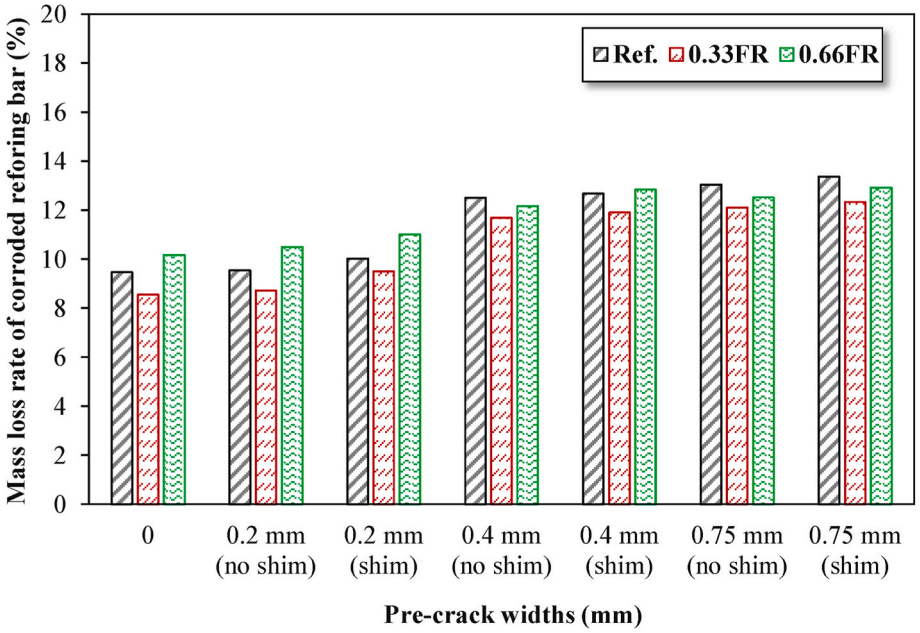

Fig. 17. Mass loss rate of reinforcing bars of three mixtures at different crack widths.

Table 5
Summary of previous studies and experiment data of corroded fiber-reinforced beams.

Ref.	Fiber type (content)	Length (mm)	Pre-crack widths (mm)	Corrosion initiation delay (%)	Residual yield load (%)	Residual ultimate load (%)	Mass loss of reinforcing bars (%)
This study	MSF (0.33–0.66%)	32–50	0	–	9-38↑	5-27↑	Max.12↓
			0.2–0.7	–	7-113↑	10-45↑	Max.9↓
[82]	SF (0.5%)	30–35	0	25-40↑	15-21↑	10-22↑	5-15↓
[47,83]				4-34↑	13-14↑	8-17↑	6-14↓
[32]				Max. 55↓	–	–	–
[82]			0.2–0.3	100-170↑	14-17↑	8-11↑	8-16↓
[47,83]			0.1–0.4	100-140↑	8-12↑	6-7↑	7-18↓
[36,84]	PP (0.1%–0.2%)	12–60	0	–	10-21↑	4-28↑	5-10↓
[85]	PE (0.75%–1.0%)	20	0	–	26-43↑	10-44↑	33-61↓
[30,86]		6	0.1–0.2	–	–	10-15↑	30-35↓

Note: Steel fibers (SF); Polypropylene fibers (PP); Polyethylene fibers (PE); MSF (a hybrid of PP and PE).

respectively. Nevertheless, in comparison to PP and PE, the incorporation of MSF (a hybrid of PE and PP) exhibited higher resistance towards the reduction in residual flexural performance, especially for the reinforced beam at a crack state. For example, the use of MSF increased the residual yield load and ultimate load of cracked beams by a maximum of 113% and 45%, respectively, compared to the plain beam, while the increased value of residual ultimate load was only 15% in the cracked beam made with PE.

3.6. Correlation of cross-section area loss rate and residual rate of flexural performance

It is well known that the flexural behavior of a beam can be significantly impacted by the corrosion of the reinforcing bar. Besides, according to Bezuidenhou and Zijl [8], the residual flexural behavior and remaining service life of reinforced concrete structures were significantly influenced by the pitting concentration corrosion of reinforcing bars. Therefore, according to Eqs. (3)–(6), quadratic relationships between the residual flexural behavior expressed in percent of that of the non-corroded beam and cross-sectional area loss rate of reinforcing bars were also established (Fig. 18(a)-(d)).

$$y_1 = -0.001x^2 - 0.50x + 81.05 \quad R^2 = 0.81 \tag{3}$$

$$y_2 = -0.001x^2 - 0.25x + 85.62 \quad R^2 = 0.65 \tag{4}$$

$$y_3 = -0.003x^2 - 0.04x + 82.40 \quad R^2 = 0.75 \tag{5}$$

$$y_4 = -0.003x^2 - 0.32x + 76.96 \quad R^2 = 0.79 \tag{6}$$

where y_5-y_8 are the residual yield load, ultimate load, flexural strength, and flexural toughness, respectively, of beams, and x is the cross-sectional area loss of reinforcing bars due to corrosion.

The R^2 in the second-order polynomial regression expressions ranged from 0.65 to 0.81, as shown in Eq. (6) through (8). Other regression expressions, including exponential regression (R^2 = 0.64–0.78), linear regression (R^2 = 0.64–0.80), logarithmic regression (R^2 = 0.43–0.60), and power regression (R^2 = 0.40–0.53), were also compared. The R^2 of the second-order polynomial was higher than other regression expressions, which demonstrated that the second-order polynomial regression analysis could be the most reasonable expression. Furthermore, the cross-sectional area loss of reinforcing bars exhibited higher values of R^2 (0.65–0.88) to predict the residual flexural behavior of reinforced beam cast with FR-SWC compared to using the mass loss rate of reinforcing bars (R^2 = 0.60–0.77). Therefore, the cross-sectional area loss rate of reinforcing bars can be used as a straightforward indicator to determine the residual flexural behavior of reinforced beam, including yield load, ultimate load, flexural strength, and flexural toughness. When the cross-sectional area loss state of the reinforcing bars is known, the proposed relationships can be used to predict the residual flexural behavior of

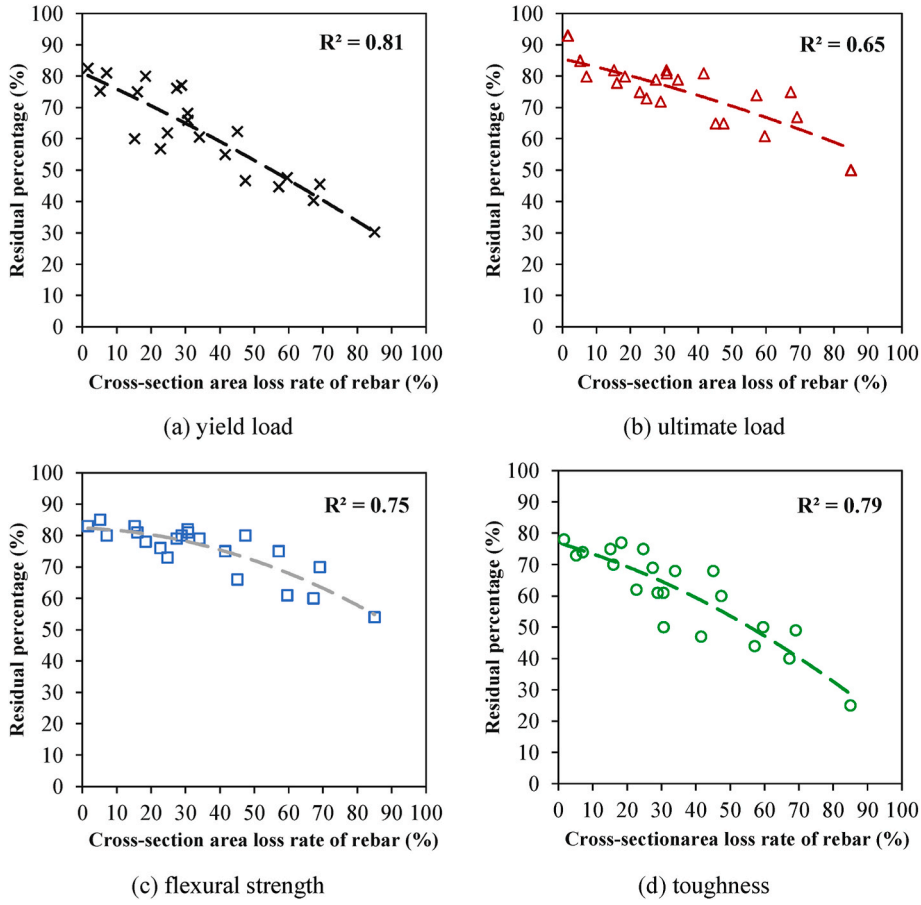

Fig. 18. Cross-sectional area loss rate versus residual percentage of flexural behavior in exposed FR-SWC beams.

exposed beams made with FR-SWC.

3.7. *Effect of MSF on residual flexural behavior of pre-crack beams*

Based on the preceding discussions, it is possible to explain the effect of MSF on the residual flexural behavior of beams subjected to corrosion. Before accelerated corrosion tests, cracks were formed on each beam during the pre-loading procedure. Fig. 19(a) depicts the pre-crack state of the no-fibrous beam, with a 0.75 mm wide crack. The crack length of notched beams without MSF approached the interface between the reinforcing bar and concrete matrix following loading. However, the growth of crack length was reduced in beams made with MSF due to the bridging effect of fibers, resulting in controlled crack length, as shown in Fig. 19(b).

Fig. 20 depicts the potential working mechanism of MSF to inhibit corrosion of reinforcing bars in shimmed MSF-reinforced beams and un-shimmed MSF-reinforced beams as compared to those in Ref. Beams. As shown in Fig. 20(a), the reduction of the cross-section of reinforcing bars caused by corrosion was higher in the cracked Ref. Beam than that of the reinforcing bar embedded in the cracked MSF reinforced beams. Such observation can explain the enhanced residual flexural performance of the cracked MSF-reinforced beam compared to the cracked Ref. Beam. This can be attributed to the effectiveness of MSF in preventing the crack length growth from reaching the surface of the reinforcing bar, thus lowering the chloride ion ingression and improving the corrosion resistance.

On the other hand, comparing Fig. 20(b)–(c) shows the extent of corrosion in the shimmed and un-shimmed MSF-reinforced beams was different. As can be seen, there was localized corrosion at the central area in the shimmed MSF-reinforced beams, while the corrosion was distributed along the reinforcing bars in the un-shimmed MSF-reinforced beams. The difference in the extent of corrosion can imply that cracks in the un-shimmed MSF-reinforced beams were partially closed due to the elastic performance of MSF, which lowered the ingression of chloride ions into the beams, leading to higher corrosion resistance. This visual observation can explain the reason for the higher residual flexural performance of un-shimmed MSF-reinforced beams compared to shimmed MSF-reinforced beams.

4. Conclusions

The objective of this study was to determine the effect of MSF volume, the initial crack width, and sustained crack width during corrosion testing on reinforcing bar corrosion. The residual flexural behavior of FR-SWC beams influenced by MSF volume and crack width after being subjected to accelerated corrosion testing was also evaluated. According to the test results, the following conclusions are warranted.

1) The use of MSF inhibited crack development and allowed the cracks to partially close after loading removal, which improved the corrosion resistance of cracked beams. The initiation of the corrosion-induced cracks in the 0.33FR and 0.66FR beams without shims was delayed by a maximum of 13% and 15%, respectively, compared to the non-fibrous beams without shims. Furthermore, the corrosion-induced crack initiation of the un-shimmed fiber-reinforced beams was delayed by 8%–20% and 12%–17% for the 0.33FR, and 0.66FR beams corresponded to similar beams with shims at the notches.
2) The use of MSF, especially at the volume of 0.66% volume, increased the residual flexural performance of cracked beams subjected to accelerated corrosion testing. The beams reinforced with 0.66% MSF

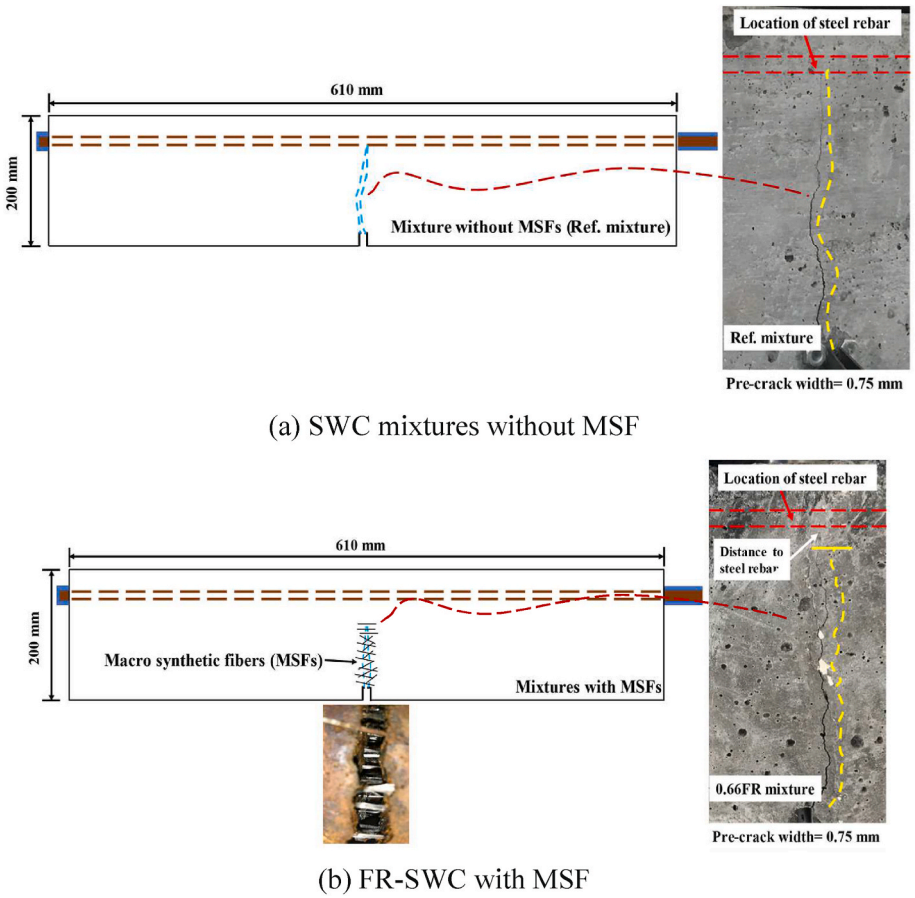

Fig. 19. Enhanced mechanism of residual flexural behavior of pre-crack beams.

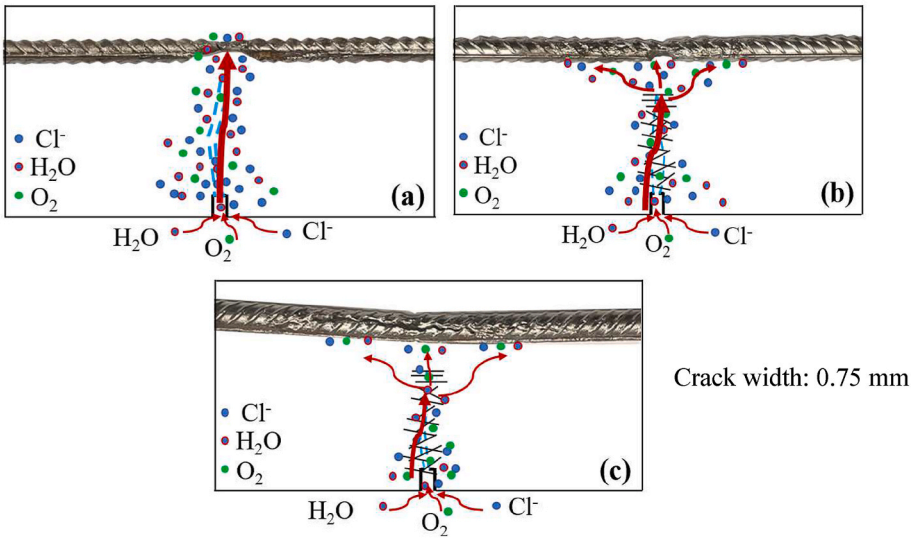

Fig. 20. Different extents of corrosion in cracked beams: (a) Ref beams; (b) shimmed MSF-reinforced beams (c) un-shimmed MSF-reinforced beams (allowed partial crack to close).

enhanced residual ultimate load, residual yield load, and residual flexural toughness by 10%–45%, 38%–113%, and 42%–150% compared to the corresponding non-fibrous beams.

3) The un-shimmed beams where cracks were allowed to partially close in FR-SWC after initial loading exhibited better residual flexural behavior compared to shimmed beams. Un-shimmed beams exhibited greater residual ultimate load, yield load, and toughness of 7%–45%, 27%–82%, and 3%–56%, respectively, compared to similar beams that with shims at the notches.
4) Crack widths lower than 0.2 mm showed no significant effect on the residual flexural behavior of beams after corrosion testing. However, the pre-crack width over 0.2 mm showed a significant influence on crack initiation and residual flexural behavior after accelerated corrosion testing. After the accelerated corrosion, the pre-cracked

beams with a 0.75-mm crack width had a residual ultimate load of 65%–76%, residual yield load of 47%–80%, and residual toughness of 38%–83%, respectively, compared to the uncracked beams.

5) Regression models with relatively high R^2 were developed between the rate of cross-sectional area loss of reinforcing bars due to corrosion and residual flexural behavior of reinforced concrete beams, which shows that the cross-sectional loss rate of the reinforcing bar is a straightforward indicator to determine the residual yield load, ultimate load, flexural strength, and flexural toughness. Furthermore, the potential working mechanism of MSF in improving the residual flexural performance of cracked beams was proposed based on the corrosion extents of reinforcing bars embedded in fiber-reinforced concrete.

Conflict of interest statements for authors

We wish to confirm that there are no known conflicts of interest associated with this publication and there has been no significant financial support for this work that could have influenced its outcome.

We confirm that the manuscript has been read and approved by all named authors and that there are no other persons who satisfied the criteria for authorship but are not listed. We further confirm that the order of authors listed in the manuscript has been approved by all of us.

We confirm that we have given due consideration to the protection of intellectual property associated with this work and that there are no impediments to publication, including the timing of publication, with respect to intellectual property. In so doing we confirm that we have followed the regulations of our institutions concerning intellectual property.

We understand that the Corresponding Author is the sole contact for the Editorial process (including Editorial Manager and direct communications with the office). He/she is responsible for communicating with the other authors about progress, submissions of revisions, and final approval of proofs. We confirm that we have provided a current, correct email address that is accessible by the Corresponding Author and which has been configured to accept email from **khayatk@mst.edu**.

Declaration of competing interest

The authors declare that they have no known competing financial interests or personal relationships that could have appeared to influence the work reported in this paper.

Data availability

Data will be made available on request.

Acknowledgment

The authors acknowledge the financial support provided by the RE-CAST University Transportation Center at Missouri University of Science and Technology (Project Number: 00062318) and GCP Applied Technologies (Project Number: 00064859). The valuable cooperation of the Center for Infrastructure Engineering Studies (CIES) and Jason Cox, Senior Research Specialist at the CIES, is greatly appreciated.

References

[1] N. Mikanovic, A. Leclerc, A. Ponge, K.H. Khayat, Workability characteristics and performance criteria for design and control of super workable concrete, in: 6th International RILEM Symposium on SCC and 4th North American Conference on the Design and Use of SCC, 2010, pp. 527–573. Montreal, Canada.

[2] F. Kassimi, Development and Performance of Fiber Reinforced Self-Consolidating Concrete for Repair Applications, University of Sherbrooke, 2013.

[3] K.H. Khayat, Abdelrazik Ahmed, Field Implementation of Super-workable Fiber-Reinforced Concrete for Infrastructure Construction, U.S. Department of Transportation, 2020. https://rosap.ntl.bts.gov/view/dot/54643.

[4] F. Kassimi, K.H. Khayat, Development of methodology to evaluate passing ability and test sample preparation for superworkable concrete, Construct. Build. Mater. 183 (2018) 356–364, https://doi.org/10.1016/j.conbuildmat.2018.06.140.

[5] F. Kassimi, K.H. Khayat, Shrinkage of high-performance fiber-reinforced concrete with adapted rheology, Construct. Build. Mater. 232 (2020), https://doi.org/10.1016/j.conbuildmat.2019.117234.

[6] K. Wang, D.C. Jansen, S.P. Shah, A.F. Karr, Permeability study of cracked concrete, Cement Concr. Res. 27 (1997) 381–393, https://doi.org/10.1016/S0008-8846(97)00031-8.

[7] M. Hoseinzade, M. Esfahani, F. Arbab, M. Shakiba, M. Yekrangnia, Residual flexural capacity of pre-cracked RC beams exposed to chloride penetration at the sea surface temperature, Construct. Build. Mater. 343 (2022), 128126, https://doi.org/10.1016/J.CONBUILDMAT.2022.128126.

[8] S.R. Bezuidenhout, G.P.A.G. van Zijl, Corrosion propagation in cracked reinforced concrete, toward determining residual service life, Struct. Concr. 20 (2019) 2183–2193, https://doi.org/10.1002/suco.201800275.

[9] S. Hong, G. Shi, F. Zheng, M. Liu, D. Hou, B. Dong, Characterization of the corrosion profiles of reinforcement with different impressed current densities by X-ray micro-computed tomography, Cem. Concr. Compos. 109 (2020), 103583, https://doi.org/10.1016/j.cemconcomp.2020.103583.

[10] L. Fan, L. Teng, F. Tang, K.H. Khayat, G. Chen, W. Meng, Corrosion of steel rebar embedded in UHPC beams with cracked matrix, Construct. Build. Mater. 313 (2021), https://doi.org/10.1016/j.conbuildmat.2021.125589.

[11] R. François, I. Khan, N.A. Vu, H. Mercado, A. Castel, Study of the impact of localised cracks on the corrosion mechanism, European J Environ Civ Eng 16 (2012) 392–401, https://doi.org/10.1080/19648189.2012.667982.

[12] L. Yu, R. François, V.H. Dang, V. L'Hostis, R. Gagné, Structural performance of RC beams damaged by natural corrosion under sustained loading in a chloride environment, Eng. Struct. 96 (2015) 30–40, https://doi.org/10.1016/J.ENGSTRUCT.2015.04.001.

[13] F. Kassimi, K.H. Khayat, Strategies to mitigate cracking of self-consolidating concrete, ACI Mater. J. 116 (2019) 73–83, https://doi.org/10.14359/51714463.

[14] A. Passuello, G. Moriconi, S.P. Shah, Cracking behavior of concrete with shrinkage reducing admixtures and PVA fibers, Cem. Concr. Compos. 31 (2009) 699–704, https://doi.org/10.1016/j.cemconcomp.2009.08.004.

[15] S. Teng, V. Afroughsabet, C.P. Ostertag, Flexural behavior and durability properties of high performance hybrid-fiber-reinforced concrete, Construct. Build. Mater. 182 (2018) 504–515, https://doi.org/10.1016/j.conbuildmat.2018.06.158.

[16] S.-J. Lee, J.-P. Won, Flexural behavior of precast reinforced concrete composite members reinforced with structural nano-synthetic and steel fibers, Compos. Struct. 118 (2014) 571–579, https://doi.org/10.1016/j.compstruct.2014.07.042.

[17] M.G. Falara, A.K. Thomoglou, F.I. Gkountakou, A. Elenas, C.E. Chalioris, Hybrid smart cementitious materials incorporating ladder scale carbon fiber reinforcement: an experimental investigation, Case Stud. Constr. Mater. 18 (2023) 1–13, https://doi.org/10.1016/j.cscm.2023.e02035.

[18] J.D. Ríos, J. Mínguez, A. Martínez-De, L. Concha, M. Ángel Vicente, H. Cifuentes, Microstructural analyses of the addition of PP fibres on the fracture properties of high-strength self-compacting concrete by X-ray computed tomography, Construct. Build. Mater. 261 (2020) 1–11, https://doi.org/10.1016/j.conbuildmat.2020.120499.

[19] C. Xie, M. Cao, M. Khan, H. Yin, J. Guan, Review on different testing methods and factors affecting fracture properties of fiber reinforced cementitious composites, Construct. Build. Mater. 273 (2021) 1–27, https://doi.org/10.1016/j.conbuildmat.2020.121766.

[20] P. Smarzewski, Influence of basalt-polypropylene fibres on fracture properties of high performance concrete, Compos. Struct. 209 (2018) 23–33, https://doi.org/10.1016/j.compstruct.2018.10.070.

[21] M.T. Kazemi, H. Golsorkhtabar, M.H.A. Beygi, M. Gholamitabar, Fracture properties of steel fiber reinforced high strength concrete using work of fracture and size effect methods, Construct. Build. Mater. 142 (2017) 482–489, https://doi.org/10.1016/j.conbuildmat.2017.03.089.

[22] M.E. Voutetaki, M.C. Naoum, N.A. Papadopoulos, C.E. Chalioris, Cracking diagnosis in fiber-reinforced concrete with synthetic fibers using piezoelectric transducers, Fibers 10 (2022) 1–23, https://doi.org/10.3390/fib10010005.

[23] A.C. Mpalaskas, T.E. Matikas, D.G. Aggelis, N. Alver, Acoustic emission for evaluating the reinforcement effectiveness in steel fiber reinforced concrete, Appl. Sci. 11 (2021) 1–13, https://doi.org/10.3390/app11093850.

[24] D.G. Aggelis, A.C. Mpalaskas, T.E. Matikas, Acoustic Monitoring for the Evaluation of Concrete Structures and Materials, Acoustic Emission (AE) and Related Non-destructive Evaluation (NDE) Techniques in the Fracture Mechanics of Concrete: Fundamentals and Applications, 2015, pp. 269–286, https://doi.org/10.1016/B978-1-78242-327-0.00013-1.

[25] S.C. Paul, S. Pirskawetz, G.P.A.G. Van Zijl, W. Schmidt, Acoustic emission for characterising the crack propagation in strain-hardening cement-based composites (SHCC), Cement Concr. Res. 69 (2014) 19–24, https://doi.org/10.1016/j.cemconres.2014.12.003.

[26] W.J. Long, Z. Wu, K.H. Khayat, J. Wei, B. Dong, F. Xing, J. Zhang, Design, dynamic performance and ecological efficiency of fiber-reinforced mortars with different binder systems: ordinary Portland cement, limestone calcined clay cement and alkali-activated slag, J. Clean. Prod. 337 (2022), 130478, https://doi.org/10.1016/J.JCLEPRO.2022.130478.

[27] Chenyu Wang, Jingjie Wei, Wu-jian Long, Biqin Dong, Review on the effect of fiber orientation distribution on mechanical performance of cement-based composites and its evaluated methods, Mater Rep 36 (2022) 1–13.

[28] J. Wei, J. Liu, K.H. Khayat, W.J. Long, Synergistic effect of HEDP.4Na and different induced pouring angles on mechanical properties of fiber-reinforced alkali-

activated slag composites, Fibers 11 (2023) 1–19, https://doi.org/10.3390/fib11030023.
[29] V. Marcos-Meson, A. Michel, A. Solgaard, G. Fischer, C. Edvardsen, T.L. Skovhus, Corrosion resistance of steel fibre reinforced concrete - a literature review, Cement Concr. Res. 103 (2018) 1–20, https://doi.org/10.1016/J.CEMCONRES.2017.05.016.
[30] C.G. Berrocal, K. Lundgren, I. Löfgren, Corrosion of steel bars embedded in fibre reinforced concrete under chloride attack: state of the art, Cement Concr. Res. 80 (2016) 69–85, https://doi.org/10.1016/J.CEMCONRES.2015.10.006.
[31] R. Roque, N. Kim, B. Kim, G. Lopp, Durability of Fiber-Reinforced Concrete in Florida Environments, 2009. Gainesville, FL.
[32] B. Kim, A.J. Boyd, J.Y. Lee, Effect of transport properties of fiber types on steel reinforcement corrosion, J. Compos. Mater. 45 (2011) 949–959, https://doi.org/10.1177/0021998310380286.
[33] P. Kotecha, A. Abolmaali, Macro synthetic fibers as reinforcement for deep beams with discontinuity regions: experimental investigation, Eng. Struct. 200 (2019), 109672, https://doi.org/10.1016/J.ENGSTRUCT.2019.109672.
[34] A.R. Al-Alawi, M.A. Mashrei, Shear capacity of sustainable ultra-high performance concrete beam reinforced with macro synthetic fiber as a sustainable alternative for stirrups and steel fiber, Case Stud. Constr. Mater. 17 (2022), e01443, https://doi.org/10.1016/J.CSCM.2022.E01443.
[35] C. Camille, O. Mirza, B. Kirkland, T. Clarke, Structural behaviour of prestressed concrete sleepers reinforced with high-performance macro synthetic fibres, Eng. Fail. Anal. 141 (2022), 106671, https://doi.org/10.1016/J.ENGFAILANAL.2022.106671.
[36] K. Bicer, H. Yalciner, A. Pekrioglu Balkıs, A. Kumbasaroglu, Effect of corrosion on flexural strength of reinforced concrete beams with polypropylene fibers, Construct. Build. Mater. 185 (2018) 574–588, https://doi.org/10.1016/j.conbuildmat.2018.07.021.
[37] F. Shi, T.M. Pham, H. Hao, Y. Hao, Post-cracking behaviour of basalt and macro polypropylene hybrid fibre reinforced concrete with different compressive strengths, Construct. Build. Mater. 262 (2020), https://doi.org/10.1016/j.conbuildmat.2020.120108.
[38] D. Li, S. Liu, Macro polypropylene fiber influences on crack geometry and water permeability of concrete, Construct. Build. Mater. 231 (2020), 117128, https://doi.org/10.1016/j.conbuildmat.2019.117128.
[39] M.S. Eisa, M.E. Basiouny, A.M. Youssef, Effect of macro-synthetic fibers on the drying shrinkage performance of rigid pavement, Innov Infrastruct Solut 6 (2021) 1–9, https://doi.org/10.1007/S41062-021-00577-Y.
[40] M. Ghahremannejad, M. Mahdavi, A.E. Saleh, S. Abhaee, A. Abolmaali, Experimental investigation and identification of single and multiple cracks in synthetic fiber concrete beams, Case Stud. Constr. Mater. 9 (2018), e00182, https://doi.org/10.1016/J.CSCM.2018.E00182.
[41] M. Chellapandian, A. Mani, S. Suriya Prakash, Effect of macro-synthetic structural fibers on the flexural behavior of concrete beams reinforced with different ratios of GFRP bars, Compos. Struct. 254 (2020), https://doi.org/10.1016/j.compstruct.2020.112790.
[42] M.G. Alberti, A. Enfedaque, J.C. Gálvez, A. Picazo, Recent advances in structural fibre-reinforced concrete focused on polyolefin-based macro-synthetic fibres, Mater. Construcción 70 (2020) 1–28, https://doi.org/10.3989/mc.2020.12418.
[43] ASTM C39, Standard Test Method for Compressive Strength of Cylindrical Concrete Specimens, 2020.
[44] ASTM C157, Standard Test Method for Length Change of Hardened Hydraulic-Cement Mortar and Concrete, 2017.
[45] ASTM C1760, Standard Test Method for Bulk Electrical Conductivity of Hardened Concrete, 2012.
[46] AASHTO TP 95-11, Standard Test Method for Surface Resistivity Indication of Concrete's Ability to Resist Chloride Ion Penetration, 2011.
[47] C.G. Berrocal, I. Löfgren, K. Lundgren, L. Tang, Corrosion initiation in cracked fibre reinforced concrete: influence of crack width, fibre type and loading conditions, Corrosion Sci. 98 (2015) 128–139, https://doi.org/10.1016/j.corsci.2015.05.021.
[48] C. Andrade, A. Poursaee, B. Ross, The role of cracks in chloride-induced corrosion of carbon steel in concrete-review, Corros and Mater Degrad 3 (2022) 258–269, https://doi.org/10.3390/CMD3020015.
[49] E. Chen, C.G. Berrocal, I. Löfgren, K. Lundgren, Correlation between concrete cracks and corrosion characteristics of steel reinforcement in pre-cracked plain and fibre-reinforced concrete beams, Mater. Struct. 53 (2020) 1–22, https://doi.org/10.1617/s11527-020-01466-z.
[50] ACI Committee 224, Control of Cracking in Concrete Structures, 2008.
[51] C.B. Käthler, U.M. Angst, K. Hornbostel, B. Elsener, Critical analysis of experiments on reinforcing bar corrosion in cracked concrete, ACI Mater. J. 117 (2020) 145–154, https://doi.org/10.14359/51722408.
[52] F.U.A. Shaikh, Effect of cracking on corrosion of steel in concrete, Int J Concr Struct Mater 12 (2018), https://doi.org/10.1186/s40069-018-0234-y.
[53] L.A. Alarab, B.E. Ross, A. Poursaee, Influence of transverse crack opening size on chloride-induced corrosion of steel bars in concrete, J. Bridge Eng. 25 (2020), 04020027, https://doi.org/10.1061/(ASCE)BE.1943-5592.0001555/ASSET/08492A24-49CC-4768-AB9F-B74FFEC31F1D/ASSETS/IMAGES/LARGE/BEENG-4331F07.JPG.
[54] M. Otieno, H. Beushausen, M. Alexander, Chloride-induced corrosion of steel in cracked concrete-Part I: experimental studies under accelerated and natural marine environments, Cement Concr. Res. 79 (2015) 373–385, https://doi.org/10.1016/j.cemconres.2015.08.009.
[55] ASTM G1-03, Standard Practice for Preparing, Cleaning, and Evaluating Corrosion Test Specimens, 2017.
[56] A. Çavdar, Investigation of freeze–thaw effects on mechanical properties of fiber reinforced cement mortars, Compos. B Eng. 58 (2014) 463–472, https://doi.org/10.1016/J.COMPOSITESB.2013.11.013.
[57] S. Fallah, M. Nematzadeh, Mechanical properties and durability of high-strength concrete containing macro-polymeric and polypropylene fibers with nano-silica and silica fume, Construct. Build. Mater. 132 (2017) 170–187, https://doi.org/10.1016/j.conbuildmat.2016.11.100.
[58] R. Kumar, P. Goel, R. Mathur, Suitability of concrete reinforced with synthetic fiber for the construction of pavements, in: Proceedings of the 3rd International Conference on Sustainable Construction Materials and Technologies, Kyoto, Japan., 2013, pp. 18–21, in: http://www.claisse.info/Proceedings.htm.
[59] O. Karahan, C.D. Atiş, The durability properties of polypropylene fiber reinforced fly ash concrete, Mater. Des. 32 (2011) 1044–1049, https://doi.org/10.1016/j.matdes.2010.07.011.
[60] J. Wang, Q. Dai, R. Si, S. Guo, Mechanical, durability, and microstructural properties of macro synthetic polypropylene (PP) fiber-reinforced rubber concrete, J. Clean. Prod. 234 (2019) 151–1364, https://doi.org/10.1016/J.JCLEPRO.2019.06.272.
[61] S. Kakooei, H.M. Akil, M. Jamshidi, J. Rouhi, The effects of polypropylene fibers on the properties of reinforced concrete structures, Construct. Build. Mater. 27 (2012) 73–77, https://doi.org/10.1016/J.CONBUILDMAT.2011.08.015.
[62] M. Nili, V. Afroughsabet, The long-term compressive strength and durability properties of silica fume fiber-reinforced concrete, Mater. Sci. Eng. 531 (2012) 107–111, https://doi.org/10.1016/J.MSEA.2011.10.042.
[63] V. Afroughsabet, L. Biolzi, T. Ozbakkaloglu, High-performance fiber-reinforced concrete: a review, J. Mater. Sci. 51 (2016) 6517–6551, https://doi.org/10.1007/s10853-016-9917-4.
[64] H.R. Pakravan, T. Ozbakkaloglu, Synthetic fibers for cementitious composites: a critical and in-depth review of recent advances, Construct. Build. Mater. 207 (2019) 491–518, https://doi.org/10.1016/j.conbuildmat.2019.02.078.
[65] Y. Yuan, Y. Ji, J. Jiang, Effect of corrosion layer of steel bar in concrete on time-variant corrosion rate, Mater. Struct. 42 (2009) 1443–1450, https://doi.org/10.1617/S11527-008-9464-9/FIGURES/11.
[66] D. Chen, S. Mahadevan, Chloride-induced reinforcement corrosion and concrete cracking simulation, Cem. Concr. Compos. 30 (2008) 227–238, https://doi.org/10.1016/J.CEMCONCOMP.2006.10.007.
[67] S. Hong, F. Zheng, G. Shi, J. Li, X. Luo, F. Xing, L. Tang, B. Dong, Determination of Impressed Current Efficiency during Accelerated Corrosion of Reinforcement, 2020, https://doi.org/10.1016/j.cemconcomp.2020.103536.
[68] Y. Yuan, J. Jiang, T. Peng, Corrosion process of steel bar in concrete in full lifetime, ACI Mater. J. 107 (2010) 563–568, https://doi.org/10.14359/51664042.
[69] F. Zheng, R. Jiang, B. Dong, S. Hong, Y. Zhang, G. Fang, Y. Wang, Visualization and Quantification of Water Penetration in Cement Pastes with Different Crack Sizes, 2022, https://doi.org/10.1016/j.conbuildmat.2022.127728.
[70] Y. Chen, G. Cen, Y. Cui, Comparative study on the effect of synthetic fiber on the preparation and durability of airport pavement concrete, Construct. Build. Mater. 184 (2018) 34–44.
[71] J. Cao, L. Liu, S. Zhao, Relationship between corrosion of reinforcement and surface cracking width in concrete, Adv. Civ. Eng. 2020 (2020), https://doi.org/10.1155/2020/7936861.
[72] V. Horsakulthai, S. Phiuvanna, W. Kaenbud, Investigation on the corrosion resistance of bagasse-rice husk-wood ash blended cement concrete by impressed voltage, Construct. Build. Mater. 25 (2011) 54–60, https://doi.org/10.1016/j.conbuildmat.2010.06.057.
[73] A.K. Azad, S. Ahmad, S.A. Azher, Residual strength of corrosion-damaged reinforced concrete beams, ACI Mater. J. 104 (2007) 40–47.
[74] H.-P. Chen, Residual flexural capacity and performance assessment of corroded reinforced concrete beams, J. Struct. Eng. 144 (2018) 1–11, https://doi.org/10.1061/(asce)st.1943-541x.0002144.
[75] M. Dopko, M. Najimi, B. Shafei, X. Wang, P. Taylor, B.M. Phares, Flexural performance evaluation of fiber-reinforced concrete incorporating multiple macro-synthetic fibers, Transport. Res. Rec. 2672 (2018) 1–12, https://doi.org/10.1177/0361198118798986.
[76] R. Abousnina, S. Premasiri, V. Anise, W. Lokuge, V. Vimonsatit, W. Ferdous, O. Alajarmeh, Mechanical properties of macro polypropylene fibre-reinforced concrete, Polymers 13 (2021), https://doi.org/10.3390/polym13234112.
[77] N. Hammad, A.M. ElNemr, H.E.D. Hassan, Flexural performance of reinforced Alkali-activated concrete beams incorporating steel and structural Macro synthetic polypropylene fiber, Construct. Build. Mater. 324 (2022), 126634, https://doi.org/10.1016/J.CONBUILDMAT.2022.126634.
[78] J. Wei, B. Cheng, L. Li, W.-J. Long, K.H. Khayat, Prediction of dynamic mechanical behaviors of coral concrete under different corrosive environments and its enhancement mechanism, J. Build. Eng. 63 (2023), 105507, https://doi.org/10.1016/J.JOBE.2022.105507.
[79] V. Picandet, A. Khelidj, H. Bellegou, Crack effects on gas and water permeability of concretes, Cement Concr. Res. 39 (2009) 537–547, https://doi.org/10.1016/j.cemconres.2009.03.009.
[80] R.H. Haddad, A.M. Ashteyate, Role of synthetic fibers in delaying steel corrosion cracks and improving bond with concrete, Can. J. Civ. Eng. 28 (2001) 787–793, https://doi.org/10.1139/l01-037.
[81] S.M.I.S. Zainal, F. Hejazi, F.N.A.A. Aziz, M.S. Jaafar, The synergistic effects of different types of hybridized synthetic fibers on concrete post-crack residual strength, KSCE J. Civ. Eng. 26 (2022) 131–142, https://doi.org/10.1007/s12205-021-1061-2.

[82] G.N. Gopu, A. Sofi, The influence of fiber RC beams under flexure on the chloride-induced corrosion, Case Stud. Constr. Mater. 17 (2022), https://doi.org/10.1016/j.cscm.2022.e01566.
[83] C.G. Berrocal, I. Löfgren, K. Lundgren, The effect of fibres on steel bar corrosion and flexural behaviour of corroded RC beams, Eng. Struct. 163 (2018) 409–425, https://doi.org/10.1016/j.engstruct.2018.02.068.
[84] I. Sadrinejad, R. Madandoust, M.M. Ranjbar, The mechanical and durability properties of concrete containing hybrid synthetic fibers, Construct. Build. Mater. 178 (2018) 72–82, https://doi.org/10.1016/j.conbuildmat.2018.05.145.
[85] T. Srimahachota, H. Yokota, Y. Akira, Recycled nylon fiber from waste fishing nets as reinforcement in polymer cement mortar for the repair of corroded RC beams, Materials 13 (2020), https://doi.org/10.3390/MA13194276.
[86] A. Kobayakawa, D. Homma, H. Mihashi, K. Shimozawa, Corrosion durability of fiber reinforced cementitious composites, J. Adv. Concr. Technol. 9 (2011) 159–167.